Reflectance, Illumination and Appearance

John J. McCann[a], Carinna Parraman[b], and Alessandro Rizzi[c]

[a]McCann Imaging, Belmont, MA, USA

[b]Centre for Fine Print Research, University of the West of England, UK

[c]Dip. Tecnologie dell'Informazione, Università degli Studi di Milano, Italy

1 Topics

We studied color constancy of two 3-D Color Mondrian displays made of two identical painted wooden shapes. We used on 6-chromatic, and 5-achromatic paints applied to 100+ block facets. The three-dimensional targets adds shadows and multiple reflections not found in flat Mondrians. Observers viewed one set in nearly uniform illumination [Low-Dynamic-Range(LDR)]; the other in directional non-uniform illumination [High-Dynamic-Range(HDR)]. Both 3-D Mondrians, were viewed simultaneously, side-by-side. We used two techniques to measure how well the appearances correlated with the objects' reflectances. First, observers made magnitude estimates of changes in the appearances of surfaces having identical reflectances. Second, an author painted a reproduction of the pair of Mondrians using watercolors. We measured the watercolor reflectances to quantify the changes in appearances. Both measurements give us important data on how reflectance, and illumination affect color constancy. While universal constancy generalizations about illumination and reflectance hold for flat Mondrians, they do not for 3-D Mondrians. A constant paint does not exhibit perfect color constancy, but rather shows significant shifts in lightness, hue and chroma in response to nonuniform illumination. The results show that appearance depends on the spatial information in both the illumination and reflectances of objects.

Reflectance, Illuminaion and Apperarance

2 Color Constancy and Appearance

The psychophysics of color constancy has been studied for nearly 150 years. In fact, there are a number of distinct scientific problems incorporated in the field. These studies ask observers distinctly different questions and get answers that superficially seem to be contradictory. The computational models of color constancy for colorimetry, sensation, and perception are good examples. The Optical Society of America used a pair of definitions for sensation and perception that followed along the ideas of the Scottish philosopher Thomas Reid. Sensation is 'Mode of mental functioning that is directly associated with the stimulation of the organism' (OSA, 1953). Perception is more complex, and involves past experience. Perception includes recognition of the object. It is helpful to compare and contrast these terms in a single image to establish our vocabulary as we progress from 18th century philosophy to 21st century image processing. Figure 13-1 is a photograph of a raft, -- a swimming float -- in the middle of a lake (McCann and Houston 1983, McCann 2000). The photograph was taken in early morning: the sunlight fell on one face of the raft, while the skylight illuminated the other face. The sunlit side reflected about 10 times more 3000°K light than the 20,000°K skylight side. The two faces had very different radiances, and hence very different colorimetric values.

Figure 13-1. Photograph of raft.

For sensations, observers imagined selecting the colors they see from a lexicon of color samples, such as the Munsell Book or the catalog of paint samples from the hardware store. The question for observers was to find the paint sample that a fine-arts painter would use to make a realistic rendition of the scene. Observers said that a bright white with a touch of yellow looked like the sunlit side, and a light gray with a touch of blue looked like the skylit side. The answer to the sensation question was that the two faces were similar, but different.

For the perceptions, observers selected the colors from the same catalog of paint samples, but with a different question. The perception question was to find the paint sample that a house painter would use to repaint the raft the same color. Observers

selected white paint. They recognized that the paint on the raft is the same despite different illuminations. The perception question rendered the two faces identical. In summary, the raft faces are very different, or similar, or identical depending on whether the experimenter is measuring colorimetry, or sensation, or perception. We need completely different kinds of image processing in order to model these three questions. Colorimetry models predict receptor responses; sensation models predict the color appearance; and perception models predict the observer's estimate of the object's surface.

Following discussions of the raft picture, subsequent experiments asked the same question, using a slightly different vocabulary (Arend and Goldstein, 1987; Arend et. al., 1991). They found the same result. Namely, observer's responses depended on the observers' psychophysical task.

3 Color Constancy Models

Human color constancy involves the content of the scene. It depends on the reflectances of objects, the spectral content and the spatial distribution of the illumination, and the arrangement of the scene. There are a number of models of color constancy used to predict colors from the array of radiances coming to the eye, or the camera. They not only use a variety of image processing assumptions, they have different sets of required information, and different goals for the model to calculate. Table 13-1 lists the names of 5 types of models, their goals (result of the calculation), their required information (inputs to calculation), and references. (Table 13-1, row 1).

Retinex

Land's Color Mondrian (Land and McCann 1971a) used a flat array of matte colored papers. He varied the amounts of uniform R, G, and B illumination over the entire array of more than 100 papers. He measured the light coming from a paper, then moved to a second paper and changed the illumination so that the second paper sent the same stimulus at a pixel to the eye. This experiment demonstrated that identical retinal stimuli generate all colors. A red paper still looked red when its illumination was altered so that it was the same light stimulus as a green paper. The quanta catch of the retina at a pixel does not correlate with appearance. Color constancy measurements showed that color appearance correlates with the scaled integrated reflectance of the paper in Land's Color Mondrian (McCann et al. 1976). This work calculated the paper's appearance using spatial comparisons. Further, it showed that the spatial comparison model predicted observer matches. The measured discrepancies from perfect constancy were predicted by crosstalk between the cone sensitivity spectra.

Land's Retinex model simply requires, as input, the spectral radiances at each pixel in the field of view. Its goal is to calculate the appearance of all colors in the scene. It builds color appearances out of spatial comparisons. Land said '... the function of

retinex theory is to tell how the eye can ascertain reflectance in a field in which the illumination is unknowable and the reflectance is unknown.' (Land and McCann 1971). Later retinex papers restated the language using edges and gradients, instead of illumination and reflectance. This was a result of studies of real life scenes in which: gradients in reflectance are difficult to see, and shadows with abrupt edges in illumination are highly visible (McCann 1999, 2004) (Table 13-1, row 2).

Color Constancy: 5 Types of Models

Model	Calculation Goal [Output]	Given Information [Model Input]	Reference
Retinex	appearance (sensation)	radiance array of entire scene	Land & McCann, 1971
Discount Illumination CIELAB and CIECAM	appearance (sensation)	pixel's radiance + pixel's irradiance	CIELAB, 1976 CIECAM, 2004
Computer Vision	reflectance	radiance array of entire scene	Ebner, 2007
Surface Perception	reflectance perception	radiance array + adaptation	Brainard & Maloney, 2004
Spatial Color Synthesis Algorithms	appearance (sensation)	radiance array of entire scene	Rizzi & McCann, 2007

Table 13-1 lists five classes of color constancy models. The first two columns list the names and the goals of the model's calculation. The third column identifies the information from the scene required to do the calculation. The fourth column lists references that describe the details of the calculation.

CIELAB and CIECAM

In the late 19th century, discussions of constancy began with the appearances of objects in different spectral illuminations. In 1872 Hering wrote 'The approximate constancy of the colors of seen objects, in spite of large quantitative or qualitative changes of the general illumination of the visual field, is one of the most noteworthy and most important facts in the field of physiological optics. Without this approximate constancy, a piece of chalk on a cloudy day would manifest the same color as a piece of coal does on a sunny day, and in the course of a single day it would have to assume all possible colors that lie between black and white.' (Hering, 1905). Helmholtz proposed the idea that humans discount the illumination, (Helmholtz,1866) so that appearances correlated with recognizing the object, namely its reflectance. This principle is incorporated in pixel based color appearance models such as 1976 CIELAB and 2004 CIECAM (CIE, 1978; 2004).

These models use physical measurements of the illumination to normalize radiances from objects and remove the spectral information contained in the illumination. These models cannot predict color appearance without measurements of illumination at the pixel of interest as input. CIECAM requires that the user assign four scene-dependent coefficients c, Nc, FLL, and F, based on viewing conditions (Hunt, 2004). (Table 13-1, row 3).

Computer Vision

Computer Vision models work to remove the illumination measurement limitation found in CIE colorimetric standards by calculating illumination from scene data. The image processing community has adopted this approach to derive the illumination from the array of all radiances coming to the camera. Since estimating the illuminant from pixel array is a multidimensional ill-posed problem, computer vision models need to apply some constraints on the scene. These constraints can regard spectral content or geometry of the illuminant, statistic of reflectance, etc. For example, one of the assumptions used in many Gray-World algorithms, is that scenes have a constant average reflectance. If true, then Gray-World algorithms can use the average radiance of all pixels to measure the spectral distribution of the illuminant.

As long as the illumination is constant for all pixels in the scene, then each pixel's radiance divided by the calculated illumination will equal that pixel's reflectance. Computer-vision models measure success by how well they can calculate an object's reflectance in different spectral illuminants. In order to use these models in a discussion about human vision, we need to perform a separate psychophysical experiment to test whether appearances correlate with reflectance for the image in question. One should not use such models for vision in situations where appearance deviates from reflectance. These models often assume perfect color constancy which is quite different from the approximate constancy found in humans. This field has been studied by Richards, Buchsbaum, Marr, Horn, Z'Mura, Adelson, Sinha, Pentland, Funt, Drew, Finlayson, Hubel, Hordley, and many others. (Richards, 1988; Horn, 1974; Buchsbaum, 1980; Marr, 1982; Funt and Drew, 1998; Sinha and Adelson, 1993; Adelson and Pentland,1996; D'Zmura and Iverson, 1993, 1993b; Finlayson, Hubel, and Hordley, 1997; Rutherford and Brainard, 2002; Purves and Lotto, 2003) A summary of this approach is found in Ebner 2007). (Table 13-1-row 4)

Surface Perception

Surface Perception algorithms study and model the observer's ability to recognize the surface of objects. Following Hering's concern that chalk should not be mistaken for coal, the objective is predict human response to questions about recognizing an objects surface. Here the subjects are asked the house painter's question. What paint is on the surface? Techniques include the analysis of cues from specular reflections and Bayesian inference of the scene. This field has been

studied by Helson, Gilchrist, Lee, Maloney, Foster, Brainard, Freeman, Zaidi, Bloj, Ripamonti, Yang, and many others. (Helson 1947, 1964; Gilchrist, 2006: Lee, 1986; Maloney and Wandell, 1986; Bloj et al., 1999: Ripamonti et al., 2004; Yang and Maloney, 200; Yang and Shevell, 2003: Brainard and Maloney, 2004; Smithson and Zaidi, 2004; Brainard et.al., 2006; Foster et. al., 2009, Helson, 1947, 1964; believed that the complex visual image generated a ' pooled effect of all stimuli' , to which the organism was ' attuned or adapted' . Helson's level of reference is centrally stored and used as reference for all judgments Many elements of the visual environment are suggested to play a role in such a global normalization factor, such as visual pigment adaptation, the history of reflectances in the field of view, and temporal distribution of cues (Smithson and Zaidi 2004). See Brainard and Maloney, (2004) for summary (Table 13-1, row 4).

Spatial Color Synthesis Algorithms

The last row in the Table 13-1 cites the Spatial Color Synthesis (SCS) family of algorithms. SCSA is a term that groups together a set of algorithms derived from the Retinex model. The common point of this group is that computations build up appearances from the spatial information in the scene. They start with the quanta catch of the sensor pixel and apply spatial computations to make new image renditions, as does human vision. The SCSA family includes all the various Retinex implementations that can differ quite remarkably in the way they transform the image and apply spatial processing. They include other algorithms that recompute spatial relationships in alternative ways (e.g. ACE or RACE) [Rizzi et al. 2003, Provenzi et al. 2008]. They include image domain ratio-products, frequency based spatial filters, and bilateral filters. They all are nonlinear spatial transforms of the receptor quanta catch. In general these algorithms are applied to captured scene luminance so as to render the scene data with improved image quality. SCSA have been studied by Land, McCann, Frankle, Rizzi, Marini, Gatta, Sobol, Kotera, Hurlburt, Funt, Drew, Fairchild, Johnson, Kimmel, Elad, Durand, Casseles, Bertalmio, Provenzi, Ramponi, Jobson, Rahaman, Woodell, Morel, Belen, Susstrunk, and many others (Land and McCann 1971b, 1972, Frankle and McCann 1983; Land, 1986; Funt and Drew, 1988; Jobson et al. 1997; Rizzi et al. 2002, 2004, 2004; Gatta et al. 2006; 2007; Marini et al. 1999; Marini and Rizzi, 2000; Sobol and McCann, 2002; Sobol, 2004; Provenzi et al. 2005, 2007, 2008; Wang, Horiuchi and Kotera, 2007; Funt, et. al. 2004; Kuang et al. 2007; Hurlbert, 2002; Kimmel and Elad, 2003,; Saponara et al. 2007; Paris and Durand, 2009; Bertalmio et al.2007; Morel et al. 2009; Meylan and Susstrunk 2004, 2006, Reinhard, et al, 2006). See Rizzi and McCann 2007 for a description (Table 13-1, row 6).

All five models listed in Table 13-1 do well with their predictions in the flat uniformly illuminated Color Mondrian. The experiments in this paper present a different set of requirements for color appearance models. Here, with a restricted set of reflectances and highly variable illumination, we have more information to

help sort out the importance of reflectance and illumination, as well as edges and gradients in modeling human vision.

4 Changes in Appearance from Changes in Illumination

The experiments in this chapter are designed to study the interplay of reflectance, illumination and spatial content in human color appearance (sensation).

Figure 13-2 (left) Low-dynamic-range (LDR) scene, (right) High-dynamic-range (HDR) scene.

We replaced the flat array of color papers used in Land's Mondrian (Land and McCann, 1971a) with a collection of three-dimensional painted blocks. We replaced the 100 plus color papers used in Land's Mondrian with eleven reflectances: 6 chromatic and 5 achromatic. We replaced the spatially uniform illumination with a pair of different illuminant configurations: one as uniform as possible, and the other highly directional and with different emission spectra. The uniform illumination has a low dynamic range (LDR), while the directional one has a high dynamic range (HDR) (Parraman et. al. 2009) While Land used many reflectances to make a complex array of radiances, we used the shadows and gradients created by the 3-D objects to generate complexity. The three-dimensional nature of these test targets adds shadows and multiple reflections. These properties enrich the targets and make them more like real scenes. Here we measure the effects of illumination on constant reflectances. Human vision models can take advantage of this data to assess how well their predictions match appearances.

Two identical 3-D Mondrians

The experiment used two identical sets of objects in uniform and in non-uniform illumination in the same room at the same time. We painted each of the flat surfaces with one of eleven different paints (R, Y, G, C, B, M, W, NL, NM, ND, K). Figures 13-2 shows photographs of the two parts of the scene.

Figure 13-3 (left) shows a circular test target with 11 painted sections. Figure 13-3 (right) lists the Munsell chip closest to each paint, evaluated in daylight, and the measured Yxy in LDR light.

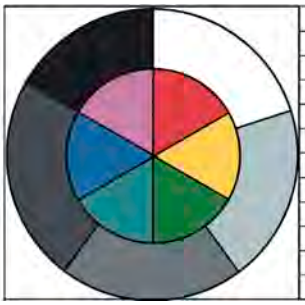

Name	Munsell	Y	x	y
R	2.5R 4/14	43.2	.631	.335
Y	2.5Y 8/14	105.0	.553	.429
G	10GY 5/12	29.7	.370	.547
C	10BG 6/8	39.9	.350	.434
B	5PB 4/12	20.6	.351	.350
M	10P 6/10	65.1	.520	.359
W	N 10/	156	.464	.417
G7.5	N 7.5/	76.3	.456	.418
G6	N 6/	44.5	.456	.418
G4	N 4/	21.2	.452	.416
K	N 1/	9.12	.462	.413

Figure 13-3 shows the flat painted test target; the paint designations, the Munsell designation and Y,x,y values

Characterization of LDR and HDR Illuminations

Above, in Figure 13-2 (left) we see a photograph of the LDR Mondrian in illumination that was as uniform as possible. The blocks were placed in an illumination cube. It had a white floor, translucent top and sides, and a black background. We directed eight halide spotlights on the sides and top of the illumination cube. The combination of multiple lamps with the same emission spectra, light-scattering cloth and highly reflective walls made the illumination nearly uniform. Departures from perfect uniformity came from shadows cast by the 3-D objects, and the open front of the cube for viewing.

Figure 13-2 (right) is a photograph of the HDR Color Mondrian illuminated by two different lights. One was a 150W tungsten spotlight place to the side of the 3-D Mondrian at the same elevation. It was placed 2 meters from the center of the target. The second light was an array of WLEDs assembled in a flashlight. It stood vertically and was placed quite close (20 cm) on the left. Although both are considered variants of white light they have different emission spectra. The placement of these lamps produced highly non-uniform illumination and increased the dynamic range of the scene (McCann, et. al., 2009a, 2009b).

In the HDR 3-D Mondrian, the black back wall had a 10 cm circular hole cut in it. Behind the hole was a small chamber with a second black wall 10 cm behind the other. We placed the flat circular test target on the back wall of the chamber. The angle of the spotlight was selected so that no direct light fell on the circular target. That target was illuminated by light reflected from the walls of the chamber. The target in the chamber had significantly less illumination than the same paints on the wooden blocks. The target in the chamber significantly increased the range of the non-uniform display. However, human observers had no difficulty seeing the darker circular target.

One way of assessing the uniformity of illumination is to make a third set of blocks, all painted middle grey. We photographed this actual Gray-World in the LDR lighting geometry (Figure 13-4, left). It shows that with 3-D objects uniform illumination is extremely difficult to achieve. Despite the use of 8 light sources and light diffusers, the three-dimensional objects cast faint shadows on other block faces. Perfectly uniform illumination requires that the object be in the center of a perfect integrating sphere. The Gray-World under HDR lighting geometry (Figure 13-4, right) shows a much wider range of luminances and apparent lightnesses.

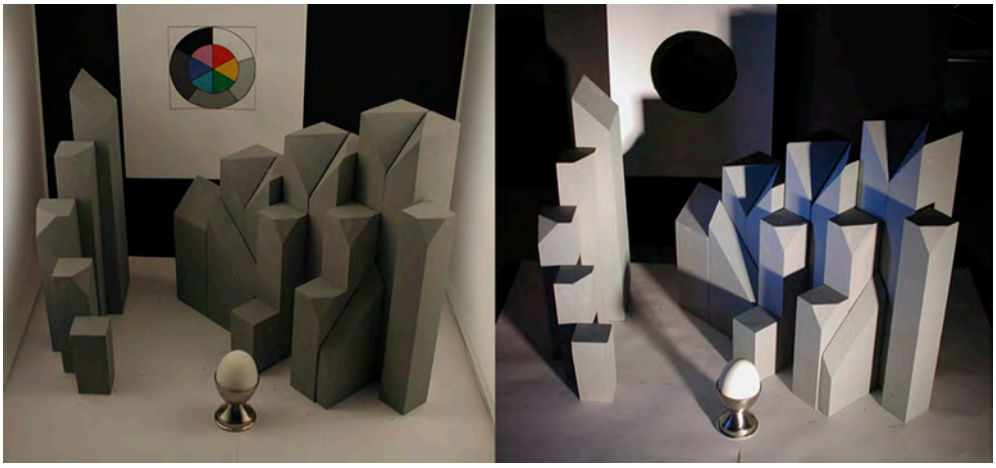

Figure 13-4 (left) LDR Gray-World 3-D Mondrian; (right) HDR. The same gray Mondrian blocks shows that directional illumination can change a pixel's radiance and appearance. The camera digits in HDR illumination are as high as 210, while in the shadows they are as low as 3.

5 Magnitude Estimation Measurements

Observers compared the HDR and LDR 3-D Mondrians (McCann, Parraman and Rizzi 2009A, 2009B). They were given a four-page form that identified a selection of 75 areas in the displays. The observers were shown the painted circular test target (Figure 13-2 left) placed on the floor of the display, in uniform light. This standard was explained to be the appearance of 'ground truth'. They were told that all the flat surfaces had the same paints as the standard.

Figure 13-5 (left) shows the ' ground truth' reflectance samples and illustrates the strategy for magnitude estimation of hue shifts; (center) lightnesses; (right) chroma.

Observers were asked if the selected areas had the same appearance as ' ground truth'. If not, they were asked to identify the direction and magnitude of the change in appearance. The observers recorded the estimates on the forms. Observers were asked to estimate hue changes starting from each of the six patches of colors [R, Y, G, C, B, M]. Participants were asked to consider the change in the hue as a percentage difference between the original hue, e.g. R, and the hue direction Y. For example, 50%Y indicates a hue shift to a color halfway between R [Munsell 2.5R] and Y [Munsell 2.5Y] (Figure 5, left). 50% Y is Munsell 2.5YR. 100%Y meant a complete shift of hue to Y. Observers estimated lightness differences on a Munsell-like scale indicating either increments and decrements, for the apparent lightness value (Figure 5 center). Observers estimated chroma by assigning paint sample estimates relative to 100% (Figure 5, right). In case the target patch appears more saturated than ' ground truth' , estimates can overtake 100%.

We measured the Munsell Notation of chips of the 11 painted ' ground truth' samples, by placing the Munsell chips on top of the paint samples in daylight. We know the direction and magnitude of changes in appearance from observer data. We made linear estimations to calculate the Munsell designation of the matching Munsell chip for each area. We used the distance in the Munsell Book as described in the MLAB color space, (Marcu, 1998; McCann, 1999b) as the measure of change in appearance. We assumed that the Munsell Book of Color is, as intended, equally spaced in color. MLAB converts the Munsell designations to a format similar to CIELAB, but avoids its large departures from uniform spacing (McCann, 1999b). When the observer reports no change in appearance from illumination MLAB distance is zero. A change as large as white to black (Munsell 10/ to Munsell 1) is MLAB distance of 90.

Figure 13-6 identifies the 101 painted facets measured in these experiments. Appendix 1 shows the average of eleven observers' results of the selected areas in the pair of 3-D Mondrians. We converted the observer magnitude estimates to an observed Munsell chip designation, and then to MLAB Color space. Munsell chips vary from less than 10 to 1, while L*a*b* varies from 100 to 0. We multiplied the estimated Munsell Lightness Value by 10.0.

$$ML = 10 * (MunsellLightnessValue) \quad (13\text{-}1)$$

$$Mb = 5 * (MunsellChroma * \sin(HueAngle * PI()/180)) \quad (13\text{-}2)$$

$$ML = \sqrt{(5 * MunsellChroma)^2 + (Mb)^2} \quad (13\text{-}3)$$

We multiplied Munsell Chroma by 5 and by the sin of the hue angle as to calculate Mb. Ma is the third side of the triangle in the Chroma plane for that Lightness (McCann, 1999b). We averaged the 11 observed ML, Ma, MB values for each chip.

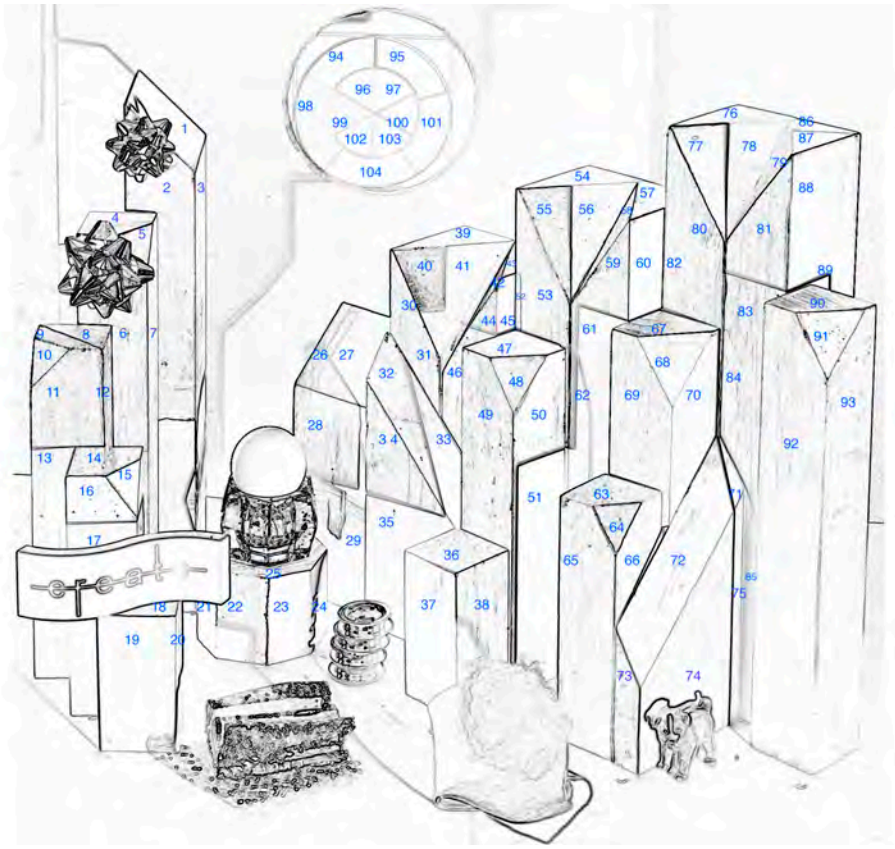

Figure 13-6. Identification of facet numbers.

Appendix 1 lists the average ML, Ma, Mb magnitude estimates for each color paint. For example, we asked the observers to evaluate 5 facets with red paint in HDR. We used the circular target in front of the display as reference; R equals 2.5R4/14. We converted this Munsell designation to ML=40, Ma=69.9, Mb=7.3 values. The red paint in the circular target on the back wall [Area 97] (See Figure 6), was ML=43.6, Ma=66.2, Mb=4.1 for LDR, and ML=27.1, Ma=59.5, Mb=6.3 for HDR. The distance between magnitude estimates was 18 MLAB units, or 20% of the distance between white and black.

Magnitude Estimate Results

Appendix 1 lists the lightness (ML), hue and chroma (Ma, Mb) for the 11 paints and the average magnitude estimates for 78 selected areas. For each area, we list the

average ML, Ma, Mb values; the change in appearance from ground truth as delta ML, delta Ma, delta Mb and distance in the Munsell Book from ground truth (distance). This distance is the square root of the sum of the squares of deltaML, deltaMa, deltaMb. Appendix 1 also lists the ranges of delta ML, delta Ma, delta Mb for each paint.

The observers reported larger departures from ground truth in the High-Dynamic-Range than in the Low-Dynamic range scenes. For the red paint the LDR ranges were ML=10, Ma=4, Mb=2; the HDR ranges were ML=18, Ma=28, Mb=45. This pattern held for all the eleven paints. For the five red samples, the individual distances in Munsell MLAB space were LDR=6, 14, 14, 11, 6 and HDR= 16, 25, 15, 6, 50. This illustrates an important point. In the LDR scene on average the changes in appearance were smaller in nearly uniform illumination. In the HDR scene the changes in appearance were larger, but there were individual areas that showed little or no change from ground truth. The changes in appearance in the LDR were mostly changes in lightness. The changes in HDR were found in both lightness and chroma. Area 11 in LDR is ML=43, Ma=65, Mb=4. This is 3 units lighter, 4 units less red, and 3 units bluer than ground truth. In HDR illumination Area 11 is a sample of red paint that is close to the LED illumination on the right. It has more short-wave light than the tungsten lamp on that side of the Mondrian. Area 11 in HDR is ML=55, Ma=48, Mb=-36; that is 15 units lighter, 22 units less red and 43 units more blue than ground truth. For this facet the departure from constancy is larger in hue than in lightness.

The yellow paint samples in Appendix 1 show that Areas 68 and 74 appear darker and have less chroma in the LDR scene (distance = 18, 22). In the HDR scene Area 74 is lighter (distance = 6), while Area 68 is 14 units lighter. Area 100 is 26 units darker in HDR.

The green samples in the LRD scene show that Area 65 is lighter (distance 20), while in HDR it is 5 units darker. In LDR areas 50 and 51 are both darker and less yellow (distance =21, 27). In HDR, Area 50 is 20 units lighter, while Area 51 is 40 units darker and 33 units bluer. Area 103 is 27 units darker and bluer in HDR.

In cyan LDR, Area 53 is 12 units lighter in both LDR and HDR. Areas 45 is about 20 units darker in both. Area 102 is 20 units darker in HDR.

In LDR all blue areas were within 10 units of ground truth. In HDR Areas 99 and 47 were darker and had less chroma (distance =30, 35).

For the blocks with white paint, the shadows in the LDR caused a drift in lightness of 30 units. In HDR Area 81 showed a distance of 1 unit. Area 83 was darker and slightly bluer (distance =33). Area 84 had light reflected from an adjacent magenta facet. It was darker and more magenta (distance 42). Area 85 had light reflected from an adjacent yellow facet. It was more yellow (distance 42).

Figure 13-7. Photograph of the painted watercolor of the LDR and HDR Mondrians.

The observer data shows that in general the color estimates in LDR are closer to ground truth than HDR. Nevertheless, there are areas in the HDR scene that look like the ground truth standard colors. The change in appearance of individual areas depends on the illumination and the other areas in the scene. The sources of illumination, the distribution of illumination, and inter-reflections of light from one facet to another, all play a part generating appearance. One cannot generalize the influence of the surface property (reflectance) of the facet on appearance. Illumination and all of its spatial properties show significant influence on the hue, lightness and chroma of observed appearances.

6 Watercolor Rendition Measurements

After observers finished the Magnitude Estimations of Munsell designations, we left the pair of 3-D Mondrians in place. One of the authors (Carinna Parraman) painted with watercolors on paper a rendition of both 3-D Mondrians (Parraman, et. al 2010). The painting took a considerable time to make the reproduction as close as possible to the appearances in both displays. Painters are usually applying their particular ' aesthetic rendering' that is a part of their personal style. In this case the painter worked to present on paper the most accurate reproduction of appearances possible. As with the magnitude estimation measurements, both LDR and HDR were viewed and painted together in the same room at the same time. Figure 13-7 is a photograph of the watercolor painting of the combined LDR/HDR scene.

We made reflectance measurements with a Spectrolino® meter in the center of 101 areas. If the same paint in the scene appeared the same to the artist, then all paintings spectra for this area should superimpose. They do not. The artist selected many different spectra to match the same paint on a number of blocks. (Figures

13-8, 13-9 and 13-9). The artist selected a narrower range of watercolor reflectances to reproduce the LDR scene. Many more paint colors are needed to reproduce the HDR scene. Nevertheless, some block facets appeared the same as ground truth, while others showed large departures.

We measured the reflectance spectra of both LDR and HDR paintings at each of the 101 locations identified in Figure 13-6 using a Spectrolino® meter. The meter reads 36 spectral bands, 10 nm apart over the range of 380 to 730 nm. We calibrated the meter using a standard reflectance tile. The average reflectance for all wavebands for the all LDR samples is 39.9%. The average reflectance for all wavebands for the all HDR samples is 32.2%. The average reflectance for all measurements is 36.0%.

We considered how to represent these reflectance measurements taking into account human vision. Analysis of percent reflectance overweights the high-reflectance readings, while analysis using log reflectance (optical density) overweights the low-reflectance values. Experiments that measure equal changes in appearance show that the cube root of reflectance is a good approximation of equal visual weighting (Wyszecki and Stiles,1982). This non-linear cube root transformation of reflectance has been shown to correlate with intraocular scatter. (Stiehl et. al., 1983; McCann and Rizzi, 2008; Rizzi and McCann, 2009) Thus, the cube root of scene luminance is a better representation of the luminance on the observers retina (McCann and Rizzi 2009). Studies by Indow (1980), Romney and Indow, (2003); Romney and D'Andrade. (2003) used the L* transform as the first step in their studies of how cones, opponent processes, and lateral geniculate cells map the perceptually uniform Munsell Color Space.

We used the L* function (equation 4) to scale Spectrolino reflectance value for each waveband in the following plots of painting spectra (Figures 13-8, 13-9, and 13-10).

$$L^* = 116 * \sqrt[1/3]{reflec\,\tan nce} - 16 \qquad (13\text{-}4)$$

Chromatic watercolor reflectances

We plotted the watercolor spectra for all reproductions of the red painted block in both the LDR and HDR scenes (Figure 13-8, top row). In the LDR reproduction, all but one of the facets had very similar measured reflectances. This showed that appearances correlated well with the objects reflectance, with one exception. In the HDR reproduction the painting had a wide variety of measured reflectances, showing that the non-uniform illumination had considerable influence on limiting color constancy.

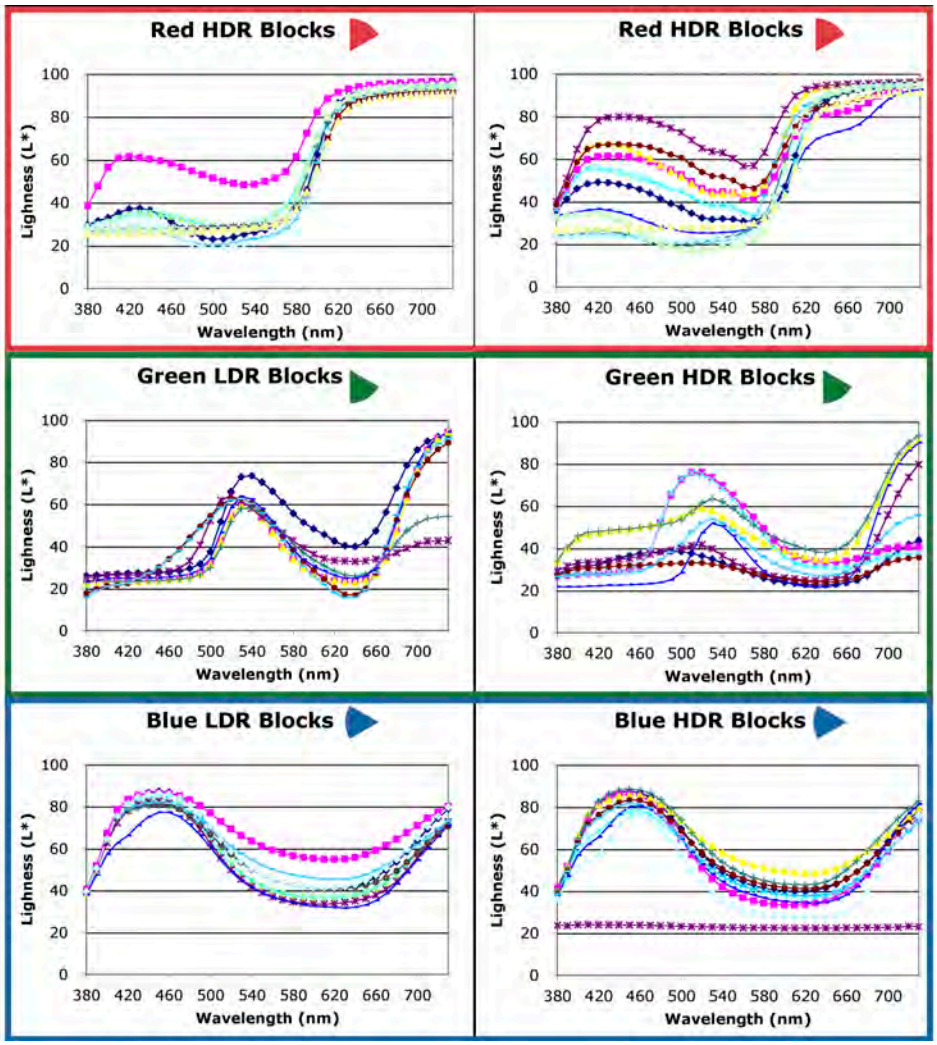

Figure 13-8. Reflectance spectra scaled by L (Lightness(L*)) of red, green, and blue, facets measured from watercolor LDR and HDR paintings.*

We plotted the watercolor spectra for all reproductions of the green painted block in both the LDR and HDR scenes Figure 13-8, second row). In both the LDR and HDR paintings, we see again a wide variety of reproduction spectra again showing that the non-uniform illumination had considerable influence on limiting colour constancy.

We plotted the watercolor spectra for all reproductions of the blue painted block in both the LDR and HDR scenes Figure 13-8, third row). In this case the HDR reproduction, had very similar measured reflectances in all but one of the facets.

The LDR reproduction had more variability in measured reflectances than the HDR painting.

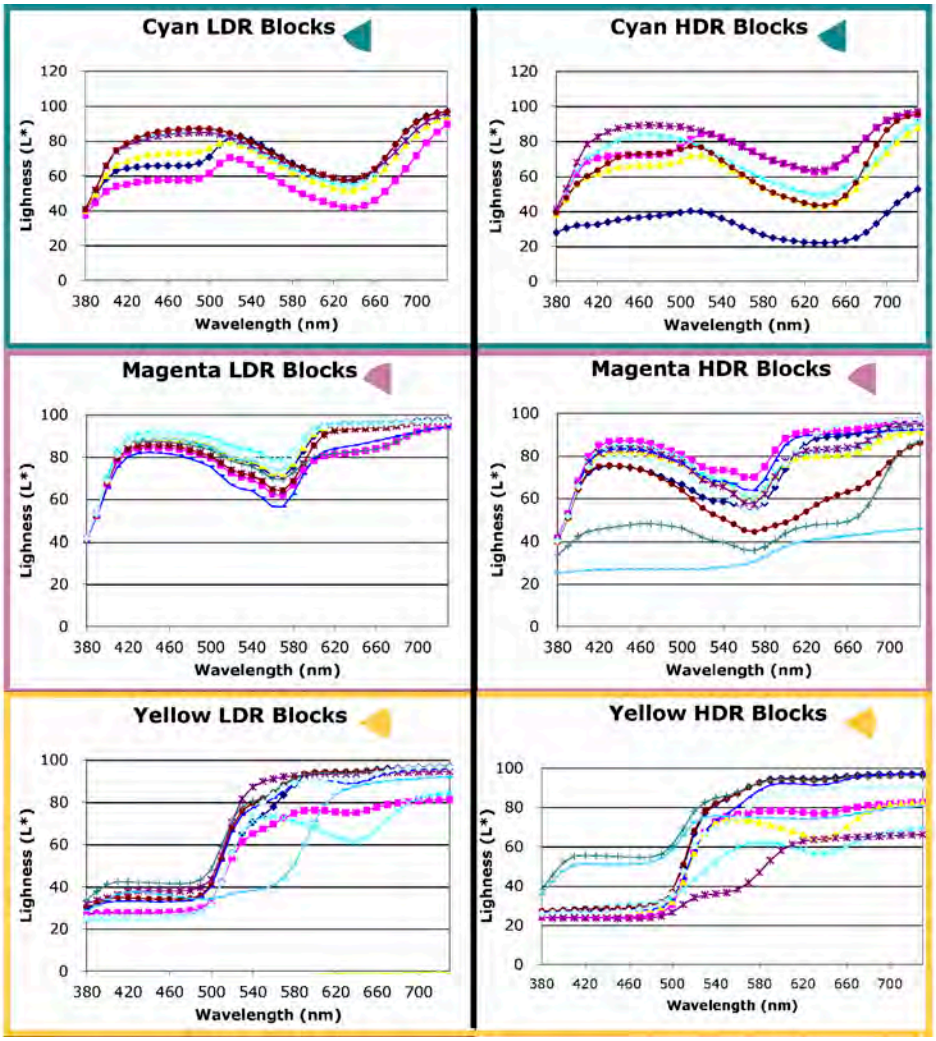

Figure 13-9 Reflectance spectra scaled by L (Lightness(L*)) of cyan, magenta, and yellow facets measured from watercolor LDR and HDR paintings.*

The cyan reproduction of the HDR scene showed greater variability in lightness of similar spectra. (Figure 13-9 first row). The magenta reproduction of the HDR scene showed greater variability in lightness and spectra. The yellow reproduction of both the LDR and HDR scene showed variability in lightness and spectra.

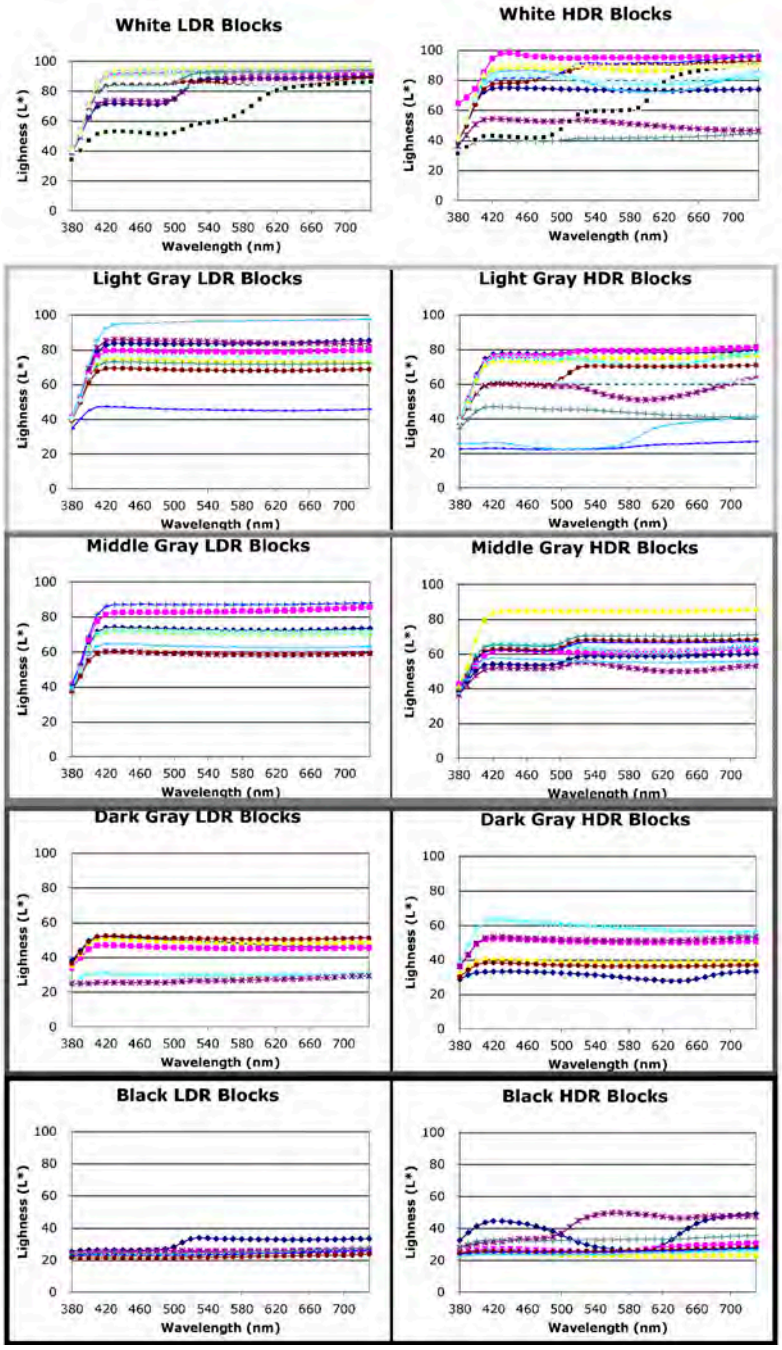

Figure 13-10 shows the reflectances of white, grays, and black facets measured from watercolor LDR and HDR paintings.

Reflectance, Illuminaion and Apperarance

It is important to study the photographs in Figure 13-2 and the paintings in Figure 13-7 to see that these results have more to do with the position of the blocks and their illumination than with the blocks' paint color.

Achromatic watercolor reflectances

Figure 13-10 compares the LDR and HRD painting reflectances for the five achromatic value blocks. Again, we see a complex pattern of departures from perfect colour constancy with significant departures caused by the specific illumination pattern. Again, the study of the photographs and paintings shows that these results have more to do with the arrangement of the blocks and their illumination than with the block's paint color.

Appendix 2 lists the three sets of colorimetric data from these experiments: reflectances of the paints on the blocks; radiances from the LDR and HDR scenes; and the reflectances of LDR/HDR watercolor rendering. For the Spectrolino measurements we integrated the reflectance spectra with CIE , $\bar{x},\bar{y},\bar{z}$ fundamentals. Then, these value were scaled by L* (equation 4) to approximate the stimulus on the retina. The left-third of Appendix 2 lists the Area Identification Number (13-6), the paint, the L*(X), L*(Y), L*(Z) for the paint on the blocks. The right third lists the corresponding values for the LDR and HDR watercolor painting. The middle of Appendix 2 lists the normalized radiance measurements made with a Konica Minolta CS100 colorimetric telephotometer. We made two measurements (Y,x,y) for each block facets. They were converted to X,Y,Z; averaged and normalized in LDR by the White paint Area 9 measurements (X=284.7, Y=247.5 cd/m2, Z=62.8); in HDR by the White paint Area 60 measurements (X=314.2, Y=273 cd/m2, Z=88.5. These normalized values were scaled by L* (equation 4).

Illumination affects lightness

Carinna Parraman's watercolor painting of the side-by-side LDR and HDR 3-D Mondrians, along with the information about the paint reflectances on the blocks, helps us to evaluate different computational models.

First, by having an artist render the appearances of the LDR / HDR scene we represent appearance in the same easily measurable physical space as the paint on the blocks. The artist's rendition converts the high-dynamic range, caused by illumination, into the set of appearances expressed in the low-dynamic range of the watercolor. The conveniently measured watercolor reflectance is a measure of appearance. These measurements are ideal for evaluating computational algorithms.

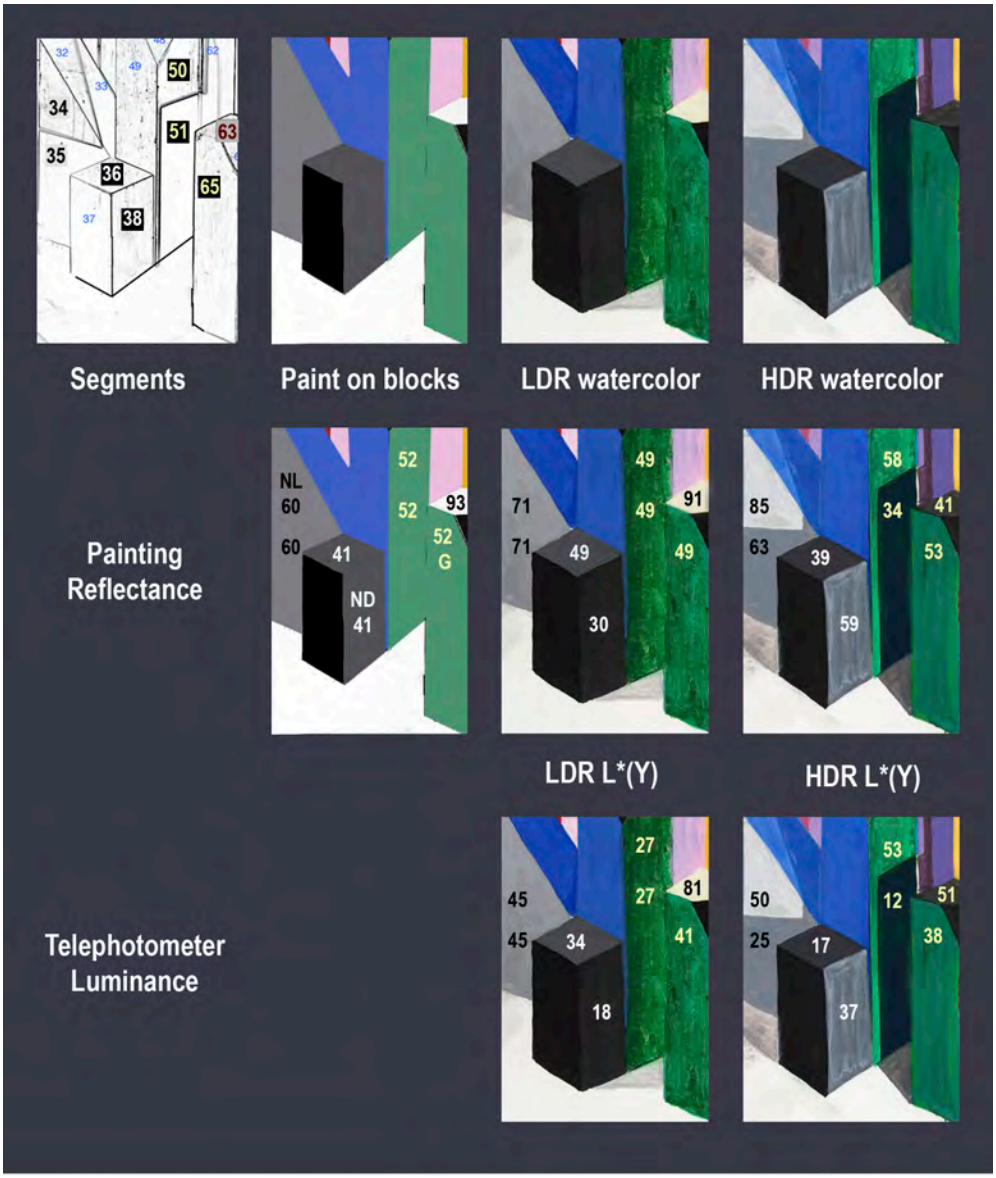

Figure 13-11 studies a region in the center of the 3-D Mondrians. The top row shows the sketch with Area IDs; the paint used on the blocks; the LDR; and HDR watercolor painting. The middle row shows the Spectrolino® watercolor L(Y) values for these block facets. The bottom row shows the telephotometer L*(Y) values for these block facets.*

Figure 13-11 shows central areas surrounding a dark gray and black block. The captured appearances of the LDR and HDR watercolor renderings have different values from the same paint on the blocks. Areas 36 and 38 have the same Neutral-

Dark (ND) paint. The paint on the block has CIE L*(Y) value for both is 41.4. These constant surface reflectances have different appearances in the LDR and HDR portions of the watercolor. In LDR area 36, the top, is lighter [L*(Y)=49] than the side [L*(Y)=30]. In HDR, the top is darker [39], than the side [59]. (See Appendix 2 for values for all 101 areas.)

In the HDR the order of the appearances changes in the different illumination. Area 38 is the lightest of the block's faces in the HDR (36, 37, 38), and nearly tied for darkest in the LDR. These changes in appearance correlate with the changes in edges caused by the different illuminations. The bottom row of Figure 13-11 shows the telephotometer scaled luminances L*(Y). The LDR area 36, the top, is lighter [34], than the side [18]. In HDR, the top is darker [17], than the side [37].

The areas in Figure 13-11 illustrate that edges caused by illumination cause substantial change in the appearance of surfaces with identical reflectances. The direction of the changes in appearance are consistent with the direction of changes in illumination on the block. Edges in illumination cause substantial changes in appearance. The data do not show correlation of appearance with luminance, rather it demonstrates that change in appearance correlates with change in luminance across edges in illumination.

Illumination affects chroma

Figure 13-12 shows a different section, right of center, of the LDR and HDR scenes. These scene portions have a tall white block face that is influenced by shadows and multiple reflections. The white paint has constant reflectance values [L*(X)=93, L*(Y)=93, L*(Z)=92)] from top to bottom (Appendix 2). The LDR appearances show light-middle-gray, and dark-middle-gray shadows.

The HDR appearances show four different appearances. The painting shows: white at the top, a blue-gray shadow below it, a pinker reflection and a yellow reflection below that. Shadows and multiple reflections show larger changes in appearance caused by different illumination.

Figure 13-12 shows sections of the watercolor for LDR (left), and HDR (right) in three sections. The top section reports the L*(X), L*(Y), L*(Z) Spectrolino measurements of the painting. The middle section reports on the photometer readings of the light coming from the blocks. The bottom section reports on the average magnitude estimates of observers in ML, Ma, Mb units.

The photographs of the LDR/HDR scene (Figure 13-2) and the watercolor painting show that the white block in LDR has achromatic shadows. The measurements shown in Figure 13-12(left) of watercolor reflectances, light from the different parts of the block, and magnitude estimates show very similar achromatic shifts in appearance. The measurement on the right side of the figure are also similar to each

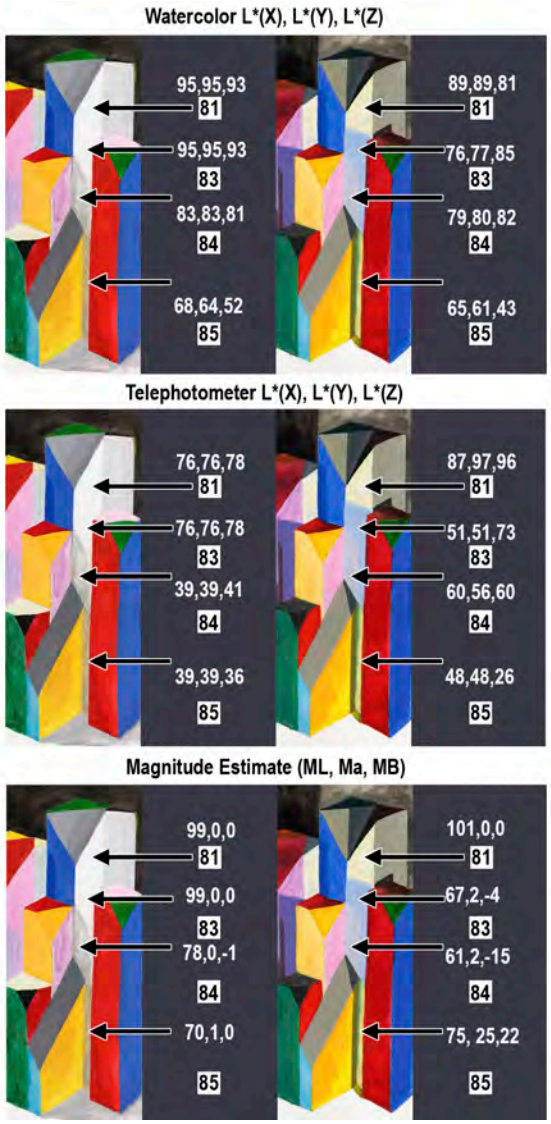

Figure 13-12 studies a region on the right of center of the 3-D Mondrians. The left image segments shows LDR watercolor and the right shows the HDR. All measurements are from a single white block with Areas 81,83,84,85. The top sections shows the watercolor reflectances [L(X), L*(Y), L*(Z)]. The middle section shows photometer readings from the blocks [L*(X), L*(Y), L*(Z)]; and the bottom section show average observer magnitude estimates [ML,Ma,Mb].*

other and indicate a chromic shift from the two light sources (Area 83) and from multiple reflections (Areas 84, 85). The changes in illumination of the single white block caused relatively sharp edges in light coming to the eye. These abrupt changes in light coming to the eye caused observers to report change in chroma as

measured by the watercolor and the magnitude estimates. Anyone familiar the history of color constancy would not think that these colors were determined with radiances from the block. However, this data supports the observation that the changes in appearance correlate with the change in radiance at these edges.

Both Figures 13-11 and 13-12 show significant inconsistencies between appearance and object reflectance. These discrepancies are examples of how the illumination plays an important role in color constancy. Both sets of measurements give very similar results. Both sets of measurements show that appearance depends on the spatial properties of illumination, as well as reflectance. Edges in illumination cause large changes in appearance, as do edges in reflectance.

7 Discussion

This paper studies a very simple question. Can illumination change the appearances of blocks with the same surface reflectance? We found a complicated answer. There is no universal generalization or result, rather a wide range of distinct individual observations. In the LDR, illumination changes appearance some of the time. In the HDR, illumination changes appearance most of the time. Appearance depends on the objects in the scene, their placement, and the spatial properties of the illuminations. In these experiments we found no evidence to support the idea that illumination has different properties from reflectance in forming appearances (sensations).

We have studied the effect of illumination using two different techniques. The magnitude estimates analyze the results in a uniform color space. By definition, distance in this space represents the size of the change in appearance for all hues, lightnesses and chromas. Here we have averaged the estimates of 11 observers for 36 facets. In the second experiment, we analyzed the watercolor painting data for 101 facets for a single observer in a modified colorimetric space. We integrated full spectral data under the color matching functions and scaled by equation 4. This color space calculates the retinal spectral response (X,Y,Z) with a correction for intraocular scatter (L*) to analyze the retinal response. Both experiments give similar results, but in different color spaces. Further, there are limitations imposed by the gamut of possible colors in the watercolor paints that do not limit the magnitude estimate experiments. The most important comparison is the effect of illumination (LDR vs. HDR) on appearance. Differences in color spaces and small differences caused by experimental techniques are of secondary importance.

Figure 13-13 plots the distribution of distances between ground truth and observed color for the measurements of appearances (sensations) using the magnitude estimates and the watercolor reflectances. The left graph binned the 38 magnitude estimates of MLAB distances into 9 groups 5 units wide. The average LDR magnitude estimate distance from ground truth was 10±8 with a maximum distance of 29.7 and a minimum of 0.7. The average HDR magnitude estimate distance from

ground truth was 18.6±6 with a maximum distance of 51.9 and a minimum of 1.0. The population LDR distances are greatest close to zero, decreasing with distance. There are no LDR distances near the maximum. The HDR has fewer near zero, with the highest population in the middle of the range. LDR and HDR have different distance distributions.

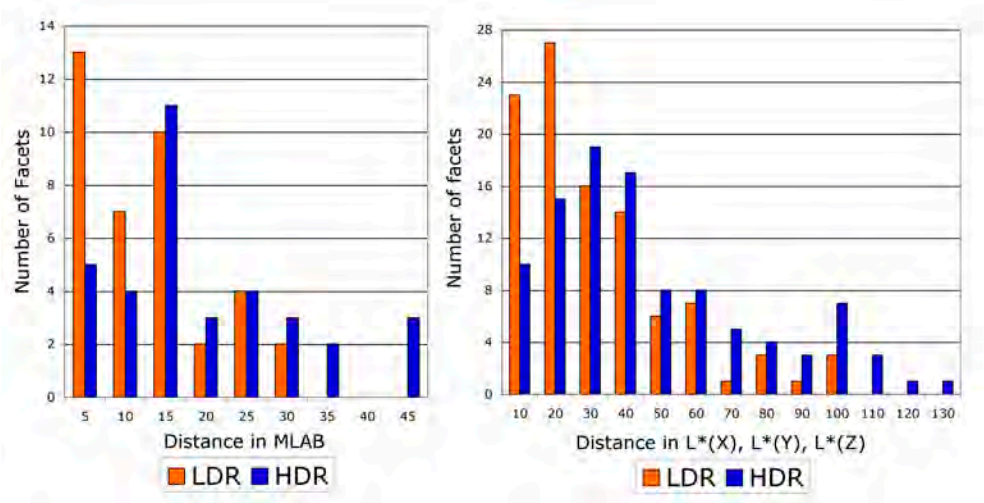

Figure 13- Comparison of the distributions of LDR and HDR distances from ground truth observed in magnitude estimation and watercolor reflectance experiments.

The right graph (Figure 13-13) binned the 101 watercolor reflectance distances [in L*(X), L*(Y), L*(Z) space] into 13 groups 10 units wide. The average LDR magnitude estimate distance from ground truth was 26.7±21.9 with a maximum distance of 95.6 and a minimum of 2.9. The average HDR magnitude estimate distance from ground truth was 42.2±29.9 with a maximum distance of 129.9 and a minimum of 1.1. Again, the population of LDR distances are greatest close to zero, decreasing with distance. There are no LDR distances near the maximum. The HDR has fewer near zero, with the highest population in the middle of the range. The magnitude estimates and watercolor reflectances show similar departures from ground truth.

Discount Illumination

Another simple question is whether observer data supports the ' discount illumination' hypothesis. Hering observed that the process was approximate. The signature of the departures from perfect constancy provides important information about how human vision achieves constancy. The data here shows that illumination alters the spatial information of the scene. Observer data correlated with spatial changes and not illumination measurements. The present experiment varies the intensities of two similar white lights. Previous experiments (McCann 2004, 2005a) varied the amounts of long-, middle-, and short-wave illumination (27

different spectra) falling on a flat surface in uniform illumination. These experiments measured the departures from perfect constancy. The results showed small changes in color appearances caused by illumination for highly colored papers, and no changes with achromatic papers. A ' discounted illuminant' must have the same effect on all papers. Thus, the departures from perfect constancy did not correlate with incomplete adaptation models. Rather, these departures correlated with changes in edge ratios seen by the broad spectral sensitivity of human cone pigments. Changing the spectral content of illumination alters the crosstalk between cone responses. Their broad spectral sensitivities alter the spatial information for colored papers, but not for achromatic ones. (McCann et al 1976, McCann 2005a). The 27 spectral illuminant data, and the data in this paper, both show that human color constancy does not work by discounting the illumination. The signatures of the departures from perfect constancy do not support that hypothesis.

Real paints and lights

In the careful analysis of reflectance and illumination there is no room for errors and artifacts introduced by image capture and display technologies. In 1976 we began to studies human vision using computer controlled complex image-displays (Frankle and McCann, 1983, McCann and Houston 1893a). Since then, we have been aware of the need for extensive calibration of electronic imaging devices. (McCann and Houston, 1983b). For the experiments in this paper, we chose to fabricate our test scene with real objects painted with exactly the same paints. We chose to use real light sources. We were able to measure the reflectance of each paint, the Y,x,y of the light coming from the surface, and the full spectra of the paints in the watercolor.

High Dynamic Range (HDR) techniques are widely used today. Multiple exposure techniques are used to improve photographic reproductions (Debevic and Malik 1997, McCann 2007). Nevertheless, multiple exposures do not record accurate scene radiances. Rather they record the sum of the scene radiance and the undesired veiling glare from the camera and its optics. Glare is image dependent, and cannot be corrected by calibration (McCann and Rizzi 2007). Scene information and glare cannot be separated without independent radiance measurements of the scene.

Similarly, there are great difficulties in error-free rendering the information in computer memory on a print, or display device. Extensive calibration of all image areas throughout the full 3-D color space are needed to avoid hardware limitations. The hardware systems that convert digits to light have many operations that alter the light coming to the eye from the expected value to a different device-dependent value. The digital image stored in computer memory is continuously sent, via a graphics card, to the display pixel (refreshed at the rate specified by the hardware). The physical characteristics of the display (spectral emission, number and size of

pixels); the time budget (refresh rate and response times), the image processing in the graphics card; and the circuitry in the display all influence the display's light output at each pixel. The amount of light output does not always correspond to image digits in computer memory. A good example is that the EMF of the display signals in the screen wiring introduces image-dependent color shifts (Feng and Daly, 2005). Hardware systems introduce image-dependent transformations of the input signals that on average improve the display's appearance (Feng and Yoshida, 2008). HDR display with two active light modulators introduce even more complexity with high-resolution LCDs and low-resolution LEDs that are integrated with complex, proprietary, spatial filtering of the image data (Seetzen, et.al., 2004). It is not a simple matter to verify the accuracy of a display over its entire light-emitting surface, for all light levels, for its entire 3-D 24-bit color space. The combination of reflectances (range=100:1), and illuminations (range=100:1) require great precision over a range of 10,000:1. Rather than calculate the combined effects of reflectances and illumination for an image-dependent display device, we chose to use real lights and paints for this analysis.

Nevertheless, these experiments are the combination of traditional object based research using paints and lights and modern digital imaging techniques. The original experiments included making HDR image capture of these scenes using a number of different cameras. Experiments on the HDR image processing are ongoing. The goal of SCSA algorithms is to mimic vision (Rizzi 2007). We are in the process of using the data from Appendix 2 to evaluate the result of the image processing.

Color Constancy Models

As one inspects the color appearances in the LDR and HDR watercolors it is evident that these color have a physical correlate. That correlate is not the XYZ values of a pixel. The correlate is the spatial relationship of XYZ values with different pixels. Darker regions of the same reflectance paint have edges created by the illumination. The appearances observed here are consistent with a model that builds colors from image structure.

If we return to the five computational models we discussed in the introduction, we can evaluate how they apply to these experiments. The McCann, McKee, and Taylor data show that flat Mondrian appearances correlated with reflectances (measured with human cone sensitivities) in uniform illumination. The model they tested built those calculated reflectances by spatial comparisons. The intent was to show that it was possible to calculate reflectances using spatial comparisons without ever finding the illumination. If one applies a spatial model to these 3-D Mondrians we would not calculate the paints' reflectances. Instead we would get a rendition of the scene that treated edges in illumination the same as edges in reflectance. The Retinex spatial model shows correlation with reflectance sometimes, (in flat Mondrians), but not all the time (in 3-D Mondrians). (Table 13-2, Row 3)

Reflectance, Illuminaion and Apperarance

CIELAB/CIECAM models measure the X, Y, Z reflectances of individual pixels and transform them into a new color space. There is nothing in the calculation that can generate different outputs from identical reflectance inputs, as frequently observed in color appearances in 3-D scenes. These models predict the same color appearance for all blocks with the same reflectance. While useful in analyzing appearances of flat scenes such as printed test targets, it does not predict appearance with shadows and multiple reflections. (Table 13-2, Row 4)

The third class of model, Computer Vision, has the specific goal of calculating the object's reflectance. The question here is whether such material recognition models have relevance to vision. If a computer vision algorithm correctly calculated cone reflectance of the flat Mondrians, then one might argue that such processes could happen in human vision (Ebner, 2007). However, the 3-D Mondrians, and other experiments show that illumination affects the observers' responses. (Rutherford and Brainard 2002, Yang and Shevell 2003). If that same computer vision algorithm correctly calculated 3-D Mondrian reflectances, then these calculations are not modeling appearances in 3-D Mondrians. Computer Vision is a distinct discipline from human vision, with very different objectives. (Table 13-2, Row 5)

The fourth class of model, Surface Perception, has the specific goal of calculating the object's estimate of the reflectance. We did not ask the observer to guess the reflectance of the facets in these experiments. We told observers that the blocks had only 11 paints, identified in the color wheel. Observers were likely to get very high correlations with actual reflectance in the LDR because the 11 paint samples were so different from each other. In the HDR illumination we would expect that there would more confusion, as shown by the appearances in Figures 13-11 and 13-12. Modeling surface perception is a distinct field from measuring the appearances (sensations) in complex 3-D scenes. Since observers give different responses, the surface perception model must have different properties (Table 13-2, Row 6).

The fifth class of model is Spatial Color Synthesis Algorithms. Their goal is to calculate the appearance (sensation question) of the LDR and HDR scenes. The goal is to create an image processing renditions of both LDR and HDR scenes for LDR prints or displays. Their common feature is the analysis of spatial information (both reflectance and illumination), so that the correlation with reflectance depends on the scene. (Table 13-2, Row 7).

We have captured multiple exposure images of the LDR and HDR parts of the 3-D Mondrian scene, and have some preliminary renditions. Our ongoing study will incorporate the data in Appendix 2 in the evaluation of the success of the algorithms. That data will help us to assess SCSA, and other models trying to mimic the human vision system. The complexity of the 3-D Mondrian scene can allow both quantitative and qualitative validation of models. Matching just the direction of all the shifts in appearance caused by the scene is a difficult task. Matching the amount of such a shift can assess the robustness of a model.

Table13-2 summarizes the following: The human visual pathway generates appearances that correlate with reflectances some of the time. Spatial models of vision use image structure to calculate appearances also correlate with reflectance some of the time. CIE models that transform reflectance into a different color space give constant output for constant input. Computer vision, if successful, always calculates reflectance. Surface Perception models calculate the answers to a different question, namely they calculate what the observer thinks is reflectance. Finally, Spatial Color Synthesis Algorithms have the goal of calculating appearance whether, or not, it corresponds to reflectance.

Color Constancy: 5 Types of Models

Model	Calculation Goal [Output]	Mechanism	[Output] = Reflectance
Human Vision	appearance (sensation)	visual pathway	depends on edges
Retinex	appearance (sensation)	build appearance from edges & gradients	depends on edges
Discount Illumination CIELAB & CIECAM	appearance (sensation)	measure reflectance stretch	always
Computer Vision	reflectance	estimate illumination to calculate surface	always
Surface Perception	reflectance perception	cues, local adaptation, Bayesian inference	depends on edges, adaptation & inference
Spatial Color Synthesis	appearance (sensation)	build output from spatial input	depends on spatial

Table 13-2 lists human vision and the five computation models of color constancy (goals, mechanism, and outputs correlation with reflectance).

Humans exhibit color constancy using scene radiances as input. The appearances they see are influenced by the spatial information in both illumination and reflectance. Measuring, or calculating reflectance, is insufficient as a model of visual appearance in real complex scenes.

8 Conclusions

Our experiments used two identical arrays of 3-D objects in uniform (LDR) and non-uniform (HDR) illumination. They were viewed in the same room at the same time. All flat facet objects have been painted with one out of a set of 11 paints. We used two different techniques to measure the appearances to observers of these constant reflectance paints. The first recorded observer magnitude estimates of change in Munsell Notation; the second measured an artist's watercolor rendition of both scenes. Both magnitude estimates and watercolor reflectances showed the same results. There is no general rule, based on illumination and reflectance, to describe the observations. Rather, we measured a great many individual departures

from perfect constancy. In nearly uniform illumination more samples appear the same as ' ground truth' than in complex HDR illumination. Even small departures from perfectly uniform illumination generate departures in appearances from reflectance. If an image-processing algorithm discounted the illumination, and succeeded in accurately calculating objects' reflectances, then that algorithm would not predict appearances in real-life scenes with complex non-uniform illumination. Edges and gradients in illumination behave the same as edges and gradients in reflectance with the same light patterns.

Acknowledgements

We would like to thank all the participants of CREATE, European Union, Framework 6 Marie Curie Conferences and Training Courses (SCF); and staff at the Centre for Fine Print Research University of the University of the West of England, Bristol; and support from the PRIN-COFIN 2007E7PHM3-003 project by Ministero dell'Università e della Ricerca, Italy; and the assistance of Alison Davis and Mary McCann.

9 References

Adelson, E. H., and Pentland, A. P. (1996). The perception of shading and reflectance, in Visual perception: Computation and psychophysics,. New York: Cambridge University Press, 409–423.

Arend, L. E., and Goldstein, R. (1987). Simultaneous con-stancy, lightness, and brightness. Journal of the Opti-cal Society of America A, 4:(12), 2281-2285.

Arend, L. E., Jr., Reeves, A., Schirillo, J., and Goldstein, R. (1991). Simultaneous color constancy: Paper with diverse Munsell values. J. Optical Society of America A, 8(4), 661-672.

Bertalmio, M., Caselles, V., Provenzi, E., and Rizzi, A. (2007). Perceptual Color Correction Through Variational Techniques IEEE Transactions on Image Processing, 16:(4), 1058-1072.

Bertalmío, M., Caselles, V., Provenzi, E, (2009). Issues About Retinex Theory and Contrast Enhancement), International Journal of Computer Vision 83(1): 101-119.

Bloj, M. G., Kersten D., and Hurlbert, A. C. (1999), Percep-tion of three-dimensional shape influences colour per-ception through mutual illumination. Nature, 402, 877-879.

Bloj, M., Ripamonti, C., Mitha, K., Hauck, R., Greenwald, S., and Brainard, D. H. (2004) An equivalent illuminant model for the effect of surface slant on perceived lightness. Journal of Vision, 4(9), 735-746, http://journalofvision.org/4/9/6/, doi:10.1167/4.9.6.

HDR and Appearance

Brainard, D. H., Longère, P., Delahunt, P. B., Freeman, W. T., Kraft, J. M., and Xiao, B. (2006). Bayesian model of human color constancy. Journal of Vision, 6(11):10,1267-1281, http://journalofvision.org/6/11/10/, doi:10.1167/6.11.10.

Brainard, D. H., and Maloney, L. T. (2004). Perception of color and material properties in complex scenes. Journal of Vision, 4(9):i, ii-iv, http://journalofvision.org/4/9/i/, doi:10.1167/4.9.i.

Buchsbaum, G. (1980). A spatial processor model for object colour perception. Journal of the Franklin Institute, 310, 1–26.

CIE (Commission Internationale de l'Eclairage) (1978). Publication 15(E-1.31) 1972, Bureau Central de la CIE, Paris. Recommendations on Uniform Color Spaces, Color-Difference Equations, Psychometric Color Terms, Supplement No. 2.

CIE (Commission Internationale de l'Eclairage) (2004). Publication 159:2004. A colour appearance model for colour management.

D'Andrade, R. and A. K. Romney, A. K. (2003), A quantitative model for transforming reflectance spectra into the Munsell color space using cone sensitivity functions and opponent process weights, PNAS, 100, 6281-6286

Debevic, P. E., and Malik, J., Recovering high-dynamic range radiance maps from photographs, ACM SIGGRAPH, 369, (1997).

D'Zmura, M., and Iverson, G. (1993a). Color constancy: I. Basic theory of two-stage linear recovery of spectral descriptions for lights and surfaces. Journal of the Optical Society of America A, 10, 2148–2165.

D'Zmura, M., and Iverson, G. (1993b). Color constancy: II. Results for two-stage linear recovery of spectral descriptions for lights and surfaces, Journal of the Optical Society of America A, 10, 2166–2180.

Ebner, M. (2007). Color Constancy, Chapter 6, (Wiley, Chichester).

Feng, X. and Daly, S. C. (2005). Improving color characteristics of LCD. in Proc. IS&T/SPIE EI, Color Imaging X: Processing, Hardcopy, and Applications, , 5667, 328-335.

Feng, X. and Yoshida, Y, (2008). Improving the Gray Tracking Performance of LCD, Proc CGIV, 327-330.

Finlayson, G. D., Hubel, P. H., and Hordley, S. (1997). Color by correlation. Proc. IS&T/SID Color Imaging Conference, 5, 6–11,

Foster DH, Marín-Franch I, Amano K, and Nascimento SM. (2009). Approaching ideal observer efficiency in using color to retrieve information from natural scenes, J Opt Soc Am A Opt Image Sci Vis.26(11):B14-24.doi: 10.1364/JOSAA.26.000B14.

Frankle, J. and J. J. McCann, J. J. (1983). Method and apparatus of lightness imaging, US Patent, 4,384,336, May 17.

Funt, B. V., and Drew, M. S. (1988). Color constancy computation in near-Mondrian scenes using a finite dimensional linear model. IEEE Comp. Vis. & Pat. Recog, Ann Arbor, MI.

Funt, B., Ciurea, F., McCann J.J., (2004). Retinex in MatLab, Journal of Electronic Imaging, 13:(1), 48-57

Gatta, C., Rizzi, A., Marini, D. (2006) Local Linear LUT Method for Spatial Color Correction Algorithm Speed-up, IEE Proceedings Vision, Image & Signal Processing, 153:(3), 357-363.

Gatta, C., Rizzi, A., and Marini, D. (2007). Perceptually inspired HDR images tone mapping with color correction, Journal of Imaging Systems and Technology, 17: (5), 285-294.

Gilchrist, A. (2006). Seeing black and white, Oxford, Oxford University Press.

Helmholtz, H. (1866). Treatise on physiological optics (J. P. C. Southall, Trans., 2nd ed., Vol. 1962). New York: Dover.

Helson, H. (1947). Adaptation-level as frame of reference for prediction of psychophysical data. Journal of the Op-tical Society of America, 60, 1-29.

Helson, H. (1964). Adaptation-level theory; an experimental and systematic approach to behavior. New York: Harper & Row.

Hering, E. (1905). Outline of a theory of light sense (L. M. Hurvich and D. Jameson, Trans Cambridge, Harvard University Press 1964.

Horn, B. K. P. (1974). Determining lightness from an image, CGIP, 3, 277-299.

Hunt, R. W. G. (2004). The Reproduction of Color, Sixth Ed. Chicheste, John Wiley and Sons.

Hurlbert, A.C., and Wolf C.J., (2002). Contribution of local and global cone-contrasts to color appearance: a Retinex-like model, Proc. SPIE Human Vis. and El. Im. VII 4662, 286-297

Indow, T. (1980). Global color metrics and color appearance systems, Color Res & Appl 5, 5–12.

Jobson, D.J., Rahman, Z., Woodell G.A. (1997). A multiscale Retinex for bridging the gap between color images and the human observation of scenes, IEEE Trans. on Im. Proc. 6:(7), 965-976.

Khang B.G., and Zaidi,Q. (2004) Illuminant color perception of spectrally filtered spotlights. Journal of Vision, 4(9),680-692, http://journalofvision.org/4/9/2/,doi: 10.1167/4.9.5.

Kimmel, R., Elad M. (2003). A variational framework for Retinex, Int. J. of Comp. Vis., 52 (1), 7-23

Land, E. H., and McCann, J. J. (1971a). Lightness and retinex theory. Journal of the Optical Society of America, 61(1), 1-11.

Land, E. H. and McCann, J. J. (1971b). Method and system for reproduction based on significant visual boundaries of original subject, U.S Patent 3,553,360, June 5.

Land, E. H., Ferrari, L. A, Kagen, S. and McCann, J. J. (1972). Image Processing system which detects subject by sensing intensity ratios, U.S. Patent 3,651,252, Mar. 21.

Land, E., An alternative technique for the computation of the designator in the retinex theory of color vision Proc. Natl. Acad. Sci. U. S. A. 83, 3078-80 (1986).

Lee, H. C. (1986). Method for computing the scene-illuminant chromaticity from specular highlights. Journal of the Optical Society of America A, 3, 1694-1699.

Maloney, L. T., and Wandell, B. A. (1986). Color constancy: A method for recovering surface spectral reflectances, Journal of the Optical Society of America A, 3, 29-33.
Maloney, L. T., and Yang, J. N. (2001). The illuminant estimation hypothesis and surface color perception. in R. Mausfeld, R and Heyer, D (Eds.), Colour perception: From light to object . Oxford: Oxford University Press, 335–358,
Marcu, G. (1998) Gamut Mapping in Munsell Constant Hue Sections, in Proc. 6th IS&T/SID Color Imaging Conference, Scottsdale, Arizona, 159 -62.
Marini, D., Rizzi, A., Rossi, M., (1999). Color Constancy Measurement for Synthetic Image Generation, Journal of Electronic Imaging, 8:(4), 394-403.
Marr, D. (1982). Vision. San Francisco: W. H. Freeman.
McCann, J. J. (1999a). Lessons learned from Mondrians applied to real images and color gamuts, Seventh Color Imaging Conference: Color Science, Systems and Applications, 7, 1-8.
McCann, J. J. (1999b). Color spaces for color mapping, J. Electronic Imaging, 8, 354-364.
McCann, J. J. (2000). Simultaneous Contrast and Color Constancy: Signatures of Human Image Processing, Chapter 6 in Color Perception: Philosophical, Psychological, Artistic, and Computational Perspectives, Vancouver, Vancouver Studies in Cognitive Studies, S. Davis, Ed, Oxford University Press, USA, 87-101.
McCann, J. J. ed, (2004a). Retinex at 40 Symposium, Journal of Electronic Imaging 13(1), 1-145.
McCann, J. J. (2004b). Capturing a black cat in shade: past and present of Retinex color appearance models, Journal of Electronic Imaging 13(1), 36-47.
McCann, J. J. (2004). Mechanism of color constancy, 12th IS&T/SID Color Imaging Conference: 12, 29-36
McCann, J. J. (2005a). Do humans discount the illuminant?, in Human Vision and Electronic Imaging X, IS&T/SPIE, San Jose, CA, USA, SPIE Proc, 5666, 9-16.
McCann, J. J. (2005b). Rendering High-Dynamic Range Images: Algorithms that Mimic Vision, in Proc. AMOS Technical Conference, US Air Force, Maui, 19-28.
McCann, J. J. (2007). Art Science and Appearance in HDR images, J. Soc. Information Display, 15, 709-719.
McCann, J. J., and Houston, K. L. (1983a). Color Sensation, Color Perception and Mathematical Models of Color Vision, in: Colour Vision. Mollon,and. Sharpe, ed., Academic Press, London, 535-544.
McCann, J. J. and Houston, K. L. (1983b) Calculating color sensation from arrays of physical stimuli, IEEE SMC-13, 1000-1007.
McCann, J. J., McKee, S. P., and Taylor, T. H. (1976). Quantitative studies in retinex theory: A comparison between theoretical predictions and observer responses to the Color Mondrian_ experiments. Vision Research, 16, 445–458.
McCann, J. J., Parraman, C. E. and Rizzi, A.(2009a) Reflectance, Illumination, and Edges in 3-D Mondrian Colour Constancy Experiments, Proceedings of the 2009 Association Internationale de la Couleur 11th Congress, Sidney

Reflectance, Illuminaion and Apperarance

McCann, J. J., Parraman, C. E., and Rizzi, A. (2009b) Reflectance, Illumination and Edges, Proc. IS&T/SID Color Imaging Conference, Albuquerque, CIC 17, 2-7.

McCann, J. J. and Rizzi, A. (2007). Camera and visual veiling glare in HDR images, J. Soc. Info. Display 15/9, 721–730.

McCann, J. J. and A. Rizzi, A. (2008). Appearance of High-Dynamic Range Images in a Uniform Lightness Space, in CGIV 2008 / MCS/08 4th European Conference on Colour in Graphics, Imaging, Terrassa, Barcelona, España, 4, 177–182.

McCann, J. J. and Rizzi, A. (2009). Retinal HDR images: Intraocular glare and object size, J. Soc. Info. Display 17/11, 913-920.

Meylan, L and Süsstrunk, S. (2004). Color image enhancement using a Retinex-based adaptive filter, Proc. IS&T Second European Conference on Color in Graphics, Image, and Vision (CGIV 2004), 2, 359-363.

Meylan. L. and Süsstrunk, (2006). S., High Dynamic Range Image Rendering Using a Retinex-Based Adaptive Filter, IEEE Transactions on Image Processing, 15: 9, 2820-2830.

Morel, J. M., Petro, A. B. and Sbert, C. (2009). Fast Implementation of Color Constancy Algorithms, Proc. IS&T/SPIE, Electronic Imaging 2009, 7241.

OSA Committee on Colorimetry. (1953), The Science of Color, Optical Society of America, Washington, DC, 377-381.

Nascimento, S. M., and Foster, D. H. (2000). Relational color constancy in achromatic and isoluminant images. Journal of the Optical Society of America A, 17, 225-231

Paris, S, and Durand, F. (2009). A Fast Approximation of the Bilateral Filter Using a Signal Processing Approach, International Journal of Computer Vision, 81:(1), 24-52. .

Parraman, C., Rizzi, A. and McCann, J. J., (2009) Colour Appearance and Colour Rendering of HDR Scenes: An Experiment, in Proc. IS&T/SPIE Electronic Imaging, San Jose, 7241-26.

Parraman, C., McCann, J. J. and Rizzi, A, (2010) Artist's colour rendering of HDR scenes in 3-D Mondrian colour-constancy experiments, in Proc IS&T/SPIE Electronic Imaging, San Jose, 7528-1.

Provenzi, E., Rizzi, A., De Carli, L., and Marini, D., (2005). Mathematical definition and analysis of the Retinex algorithm Journal of Optical Society of America A, 22.

Provenzi, E., Fierro, M., Rizzi, A., De Carli, L., Gadia, D., and Marini, D., (2007). Random Spray Retinex: a new Retinex implementation to investigate the local properties of the model IEEE Transactions on Image Processing, 16, (1), 162-171.

Provenzi, E., Gatta, C., Fierro, M., and Rizzi, A. (2008). A Spatially Variant White Patch and Gray World Method for Color Image Enhancement Driven by Local Contrast, IEEE Transactions on Pattern Analysis and Machine Intelligence, 30: (10).

HDR and Appearance

Purves, D., and Lotto, R. B. (2003). Why we see what we do: An empirical theory of vision. Sunderland, MA: Sinauer.

Reinhard, E, Ward, G, Pattanaik, S. and Debevec, P. (2006). High Dynamic Range Imaging Acquisition, Display and Image-Based Lighting (Elsevier, Morgan Kaufmann, Amsterdam, 2006), Ch 7.

Richards, W. ed.(1988). Natural Computation, Cambridge, MIT Press.

Ripamonti, C., Bloj, M., Hauck, R., Mitha, K.,Greenwald, S., Maloney, S. I., et al. (2004). Measurements of the effect of surface slant on perceived lightness. Journal of Vision, 4(9), 747–763, http://journalofvision.org/4/9/7/, doi: 10.1167/4.9.7.

Rizzi, A., Gatta, C. and Marini, D., (2003). A New Algorithm for Unsupervised Global and Local Color Correction, Pattern Recognition Letters, 24 (11), 1663-1677.

Rizzi, A., Gatta, and C., Marini, D. (2004). From Retinex to Automatic Color Equalization: issues in developing a new algorithm for unsupervised color equalization, Journal of Electronic Imaging, 13(1). 75-84.

Rizzi, A. and McCann, J. J. (2007). On the behavior of spatial models of color, in Proc. Color Imaging XII: Processing, Hardcopy, and Applications, SPIE, San Jose, SPIE Proc, 6493, 649302-649314.

Rizzi, A. and McCann, J. J. (2009). Glare-limited appearances in HDR images, J. Soc. Info. Display 17/1, 3-12.

Robilotto, R., and Zaidi, Q. (2004) Limits of lightness iden-tification for real objects under natural viewing conditions. Journal of Vision, 4(9), 779-797,http://journalofvision.org/4/9/9/, doi:10.1167/4.9.9.

Romney A K, Indow T (2003) Color Res. & Appl. 28:182–196.

Saponara, S. Fanucci, L. Marsi, S. Ramponi, G. Kammler, D. Witte, E.M. (2007). Application-Specific Instruction-Set Processor for Retinex-Like Image and Video Processing, IEEE Transactions on Circuits and Systems II: 54:7 , 596-600.

Seetzen, H., Heidrich, H.. Stuerzlinger, W., Ward, G., Whitehead, L., Trentacoste, M., Ghosh, A. and Vorozcovs, A. (2004). High dynamic range display systems, ACM Transactionsion Graphics, Vol. 23(3), 760-768

Sinha, P. and Adelson, E. H., (1993) Recovering reflectance in a world of painted polyhedra. Proc. Fourth Intl. Conf. Comp. Vision.

Smithson, H., and Zaidi, Q. (2004) Colour constancy in con-text: roles for local adaptation and levels of reference. Journal of Vision, 4(9), 693-710,http://journalofvision.org/4/9/3/, doi:10.1167/4.9.3.

Sobol,R. (2004). Improving the Retinex algorithm for rendering wide dynamic range photographs, Journal of Electronic Imaging 13(01), 65-74.

Sobol, R. and McCann, J. J. (2002) Method for variable contrast mapping of digital images, U. S Patent, Oct, 24.

Stiehl, W. A., McCann, J. J., and Savoy, R. L., (1983). Influence of intraocular scattered light on lightness-scaling experiments, J. Opt. Soc. Am., 73, 1143-1148.

Reflectance, Illuminaion and Apperarance

Yang, J. N., and Maloney, L. T. (2001). Illuminant cues in surface color perception: Tests of three candidate cues, Vision Research, 41, 2581–2600.

Yang, J. N. and Shevell, S. K. (2003). Surface color perception under two illuminants: The second illuminant reduces color constancy. Journal of Vision, 3(5):4, 369-379, http://journalofvision.org/3/5/4/, doi:10.1167/3.5.4.

Wang, L., Horiuchi, T, and Kotera, H. (2007). High Dynamic Range Image Compression by Fast Integrated Surround Retinex Model, Journal of Imaging Science and Technology 51:(1), 34-(10).

Wyszecki, G. and Stiles, W. S. (1982). Colour Science: Concepts and Methods Quantitative Data and Formulae, 2nd Ed., Chapter 6, John Wiley & Sons, New York, 486-5

HDR and Appearance

Appendix 13-1

Low Dynamic Range

ID	area#	ML mean	Ma mean	Mb mean	delta ML	delta Ma	delta Mb	MLAB distance
R1	97	43.6	66.2	4.1	4	-3	-3	6
R2	56	52.9	64.2	5.5	13	-5	-2	14
R2	55	52.9	64.2	5.5	13	-5	-2	14
R3	92	47.9	62.3	4.8	8	-7	-3	11
R4	11	43.0	65.2	4.1	3	-4	-3	6
				range	10	4	2	
	paint	80.0	52.0	46.8	paint			
Y1	100	79.6	52.5	47.3	0	1	0	1
Y2	68	67.5	39.7	42.6	-13	-12	+4	18
Y3	69	85.4	46.9	41.6	5	-5	-5	9
Y4	19	79.5	49.7	44.9	0	-2	-2	3
Y5	74	60.7	45.0	40.0	-19	-7	-7	22
				range	24	14	7	
		50.0	6.3	59.7	paint			
G1	103	56.8	6.2	58.9	7	0	-1	7
G2	50	31.3	5.1	49.4	-19	-1	-10	21
G3	51	28.2	4.6	44.3	-22	-2	-15	27
G4	65	69.5	6.0	58.1	20	0	-2	20
G5	16	51.6	6.6	59.1	2	0	-1	2
				range	44	5	12	
		60.0	39.1	8.3	paint			
C1	102	61.8	39.8	8.5	2	1	0	2
C2	53	72.3	38.5	8.2	12	-1	0	12
C3	45	39.7	35.6	11.3	-20	-4	3	21
C4	73	61.8	39.0	8.8	2	0	0	2
				range	32	5	3	
		40.0	44.6	-40.1	paint			
B1	99	42.5	45.0	-40.5	3	0	0	3
B2	47	47.6	44.8	-40.3	8	0	0	8
B3	49	50.2	44.2	-38.3	10	0	2	10
B4	33	45.0	45.3	-40.7	5	1	-1	5
				range	7	1	3	
		60.0	5.2	-49.7	paint			
M1	96	63.5	6.0	-50.1	4	1	0	4
M2	59	70.5	5.3	-50.9	10	0	-1	11
M3	90	74.5	5.6	-49.2	14	0	1	14
M4	44	70.4	6.8	-52.2	10	2	-3	11
M5	70	48.2	5.1	-47.2	-12	0	2	12
M6	6	46.3	5.0	-46.8	-14	0	3	14
				range	28	2	5	
	0	100.0	0.0	0.0	paint			
G1-2	81	98.5	0.0	0.0	-1	0	0	1
G1-3	81/83	98.5	0.0	0.0	-1	0	0	1
G1-4	84	77.8	0.1	-0.5	-22	0	0	22
G1-5	85	70.3	0.5	0.4	-30	1	0	30
				range	29	1	0	
		75.0	0.0	0.0	paint			
G1-1	101	77.5	0.0	0.0	3	0	0	3
		40.0	0.0	0.0	paint			
G3-1	98	41.3	0.0	0.0	1	0	0	1
G3-2	40/41	39.3	0.0	0.0	-1	0	0	1
G3-3	36	43.6	0.5	-0.2	4	1	0	4
G3-4	38	31.9	0.7	0.1	-8	1	0	8
				range	12	1	0	

High Dynamic Range

ID	area#	ML mean	Ma mean	Mb mean	delta ML	delta Ma	delta Mb	MLAB distance
R1	97	27.1	59.5	6.3	-13	-7	-1	15
R2	56	26.5	48.0	-2.2	-13	-19	-9	25
R3	55	51.8	75.6	8.9	12	9	2	15
R4	92	44.1	70.3	6.4	4	4	-1	6
R5	11	55.0	48.1	-35.5	15	-19	-43	49
				range	18	28	45	
	paint	80.0	52.0	46.8	paint			
Y1	100	55.9	50.2	38.1	-24	-2	-9	26
Y2	68	94.4	51.5	46.4	14	-1	0	14
Y3	69	85.4	47.2	49.6	5	-5	3	8
Y4	19	80.7	48.5	44.6	1	-4	-2	4
Y5	74	85.8	51.0	46.0	6	-1	-1	6
				range	38	4	8	
		50.0	6.3	59.7	paint			
G1	103	32.4	4.2	38.9	-18	-2	-21	27
G2	50	70.0	7.7	60.9	20	1	1	20
G3	51	10.0	3.1	26.8	-40	-3	-33	52
G4	65	54.5	6.3	60.1	5	0	0	5
G5	16	62.2	8.2	54.7	12	2	-5	13
				range	60	5	34	
		60.0	39.1	8.3	paint			
C1	102	39.8	28.6	5.0	-20	-10	-3	23
C2	53	72.1	40.1	8.5	12	1	0	12
C3	45	74.6	35.8	19.4	15	-3	11	19
C4	73	61.5	38.7	8.2	1	0	0	2
				range	35	11	14	
		40.0	44.6	-40.1	paint			
B1	99	17.3	29.3	-28.1	-23	-15	12	30
B2	47	14.0	27.8	-24.1	-26	-17	16	35
B3	49	49.6	45.6	-42.2	10	1	-2	10
B4	33	32.7	33.4	-44.3	-7	-11	-4	14
				range	36	18	20	
		60.0	5.2	-49.7	paint			
M1	96	39.1	4.5	-43.8	-21	-1	6	22
M2	59	60.5	5.2	-52.9	1	0	-3	3
M3	44	54.3	7.6	-40.6	-6	2	9	11
M4	6	63.3	14.6	-47.8	3	9	2	10
M5	90	28.8	3.2	-23.7	-31	-2	26	41
M6	70	71.6	6.1	-48.5	12	1	1	12
				range	43	10	29	
		100.0	0.0	0.0	paint			
G1-2	81	101.0	0.0	0.0	1	0	0	1
G1-3	83	67.4	2.3	-4.3	-33	2	-4	33
G1-4	84	61.3	1.7	-15.4	-39	2	-15	42
G1-5	85	75.0	24.7	22.4	-25	25	22	42
				range	42	23	26	
		75.0	0.0	0.0	paint			
G1-1	101	58.5	0.4	-2.3	-16	0	-2	17
		40.0	0.0	0.0	paint			
G3-1	98	20.6	0.0	0.0	-19	0	0	19
G3-2	64	27.0	0.0	0.0	-13	0	0	13
G3-3	38	53.7	0.0	0.0	13	0	0	13
				range	32	0	0	

Reflectance, Illuminaion and Apperarance

Appendix 2-1

		Paint Sample			Scene Radiance						Painting								
			Spectrolino		3-D Mondrians LDR KM100			3-D Mondrians HDR KM100				LDR Watercolor Spectrolino			HDRWatercolor Spectrolino		
Paint	Area	L*(X)	L*(Y)	L*(Z)	L*(X)	L*(Y)	L*(Z)	L*(X)	L*(Y)	L*(Z)	Paint	Area	L*(X)	L*(Y)	L*(Z)	L*(X)	L*(Y)	L*(Z)
R	7	60.5	49.1	35.9	46.7	36.6	23.4	41.6	32.8	28.1	R	7	61.0	47.5	33.3	56.0	45.3	46.3
R	10	60.5	49.1	35.9	90.6	77.2	59.7	48.1	40.8	50.9	R	10	74.0	63.9	58.8	61.6	53.9	59.8
R	11	60.5	49.1	35.9	57.5	46.4	30.7	56.8	48.5	65.1	R	11	62.8	50.7	33.8	69.9	58.9	63.6
R	13	60.5	49.1	35.9	57.5	46.4	30.7	34.2	28.8	46.0	R	13	62.8	50.7	33.8	57.7	48.2	52.2
R	30	60.5	49.1	35.9	58.2	46.4	29.5	55.8	46.7	59.7	R	30	57.2	45.7	27.4	78.6	71.5	78.3
R	31	60.5	49.1	35.9	58.2	46.4	29.5	40.8	35.4	54.7	R	31	57.2	45.7	27.4	66.4	59.6	65.8
R	55	60.5	49.1	35.9	58.4	47.1	31.4	65.9	52.3	35.3	R	55	60.7	48.7	27.7	57.3	44.3	23.8
R	56	60.5	49.1	35.9	58.4	47.1	31.4	23.8	19.3	26.0	R	56	60.7	48.7	27.7	47.4	38.1	33.2
R	66	60.5	49.1	35.9	38.2	29.9	18.7	82.9	66.5	39.5	R	66	58.0	44.7	25.9	61.9	48.3	23.5
R	67	60.5	49.1	35.9	51.2	41.0	28.0	45.9	40.3	37.0	R	67	57.9	44.0	28.5	53.5	41.6	22.8
R	92	60.5	49.1	35.9	52.8	44.1	16.3	67.6	53.6	36.7	R	92	62.0	49.4	27.2	56.8	42.7	28.7
R	97	60.5	49.1	35.9	58.4	46.9	30.2	9.3	5.9	3.6	R	97	55.9	44.7	26.0	51.0	41.1	27.7
Y	19	81.5	77.4	26.6	55.0	52.6	24.2	58.3	56.3	22.3	Y	19	82.7	76.1	28.7	85.7	81.6	29.6
Y	20	81.5	77.4	26.6	56.4	53.8	26.5	51.9	50.0	23.3	Y	20	68.8	65.5	28.6	71.6	69.3	25.4
Y	43	81.5	77.4	26.6	69.9	67.0	27.2	29.9	32.5	45.0	Y	43	63.8	64.1	26.7	55.7	53.8	30.1
Y	54	81.5	77.4	26.6	75.7	72.5	29.6	19.5	18.3	14.0	Y	54	86.2	83.6	38.9	50.3	44.1	23.9
Y	68	81.5	77.4	26.6	55.3	53.0	20.7	98.1	94.2	33.2	Y	68	85.1	80.8	35.4	85.3	81.6	30.3
Y	69	81.5	77.4	26.6	74.5	71.6	29.6	81.2	79.7	46.9	Y	69	85.2	81.4	42.7	87.1	84.6	55.5
Y	74	81.5	77.4	26.6	43.9	40.9	15.2	103.3	99.0	34.0	Y	74	81.8	78.0	34.2	82.1	76.7	28.1
Y	75	81.5	77.4	26.6	31.1	29.8	14.3	46.4	44.2	12.3	Y	75	63.7	53.3	36.3	71.4	71.9	51.6
Y	100	81.5	77.4	26.6	73.0	69.2	28.6	13.2	12.1	2.7	Y	100	82.0	77.0	26.7	78.5	73.4	28.3
G	14	42.1	51.7	33.4	46.5	54.0	40.8	31.7	30.9	41.4	G	14	51.6	58.4	29.4	28.2	31.1	36.2
G	16	42.1	51.7	33.4	25.3	31.6	23.9	29.8	40.8	39.2	G	16	34.6	42.7	25.0	46.3	59.2	37.8
G	17	42.1	51.7	33.4	25.3	31.6	23.9	13.9	18.8	20.7	G	17	34.6	42.7	25.0	43.9	49.1	49.4
G	50	42.1	51.7	33.4	24.6	27.3	23.0	41.8	52.7	40.8	G	50	40.4	49.0	30.3	44.3	57.8	38.2
G	51	42.1	51.7	33.4	24.6	27.3	23.0	10.3	12.1	18.5	G	51	40.4	49.0	30.3	30.0	33.7	35.9
G	65	42.1	51.7	33.4	34.0	41.1	31.9	29.2	37.8	28.5	G	65	37.5	48.6	33.8	47.9	53.2	49.5
G	76	42.1	51.7	33.4	35.6	43.2	34.5	14.8	16.0	16.4	G	76	38.3	44.8	24.9	27.8	29.7	31.9
G	91	42.1	51.7	33.4	25.5	34.3	32.1	43.8	55.8	37.5	G	91	38.2	46.7	26.7	30.4	37.2	23.6
G	103	42.1	51.7	33.4	30.8	38.8	28.3	2.4	4.4	3.8	G	103	36.3	47.6	33.4	35.3	42.2	30.4
C	39	54.2	62.2	67.7	45.9	52.7	66.4	14.0	16.0	31.5	C	39	66.4	71.9	65.7	28.5	32.4	35.6
C	45	54.2	62.2	67.7	23.4	27.5	41.4	52.9	60.7	81.5	C	45	52.8	58.7	57.0	70.8	75.4	71.9
C	52	54.2	62.2	67.7	30.4	36.1	50.2	44.7	53.4	79.1	C	52	63.3	68.8	71.8	55.3	61.0	65.2
C	53	54.2	62.2	67.7	46.6	53.4	67.7	51.0	58.9	102.5	C	53	67.3	72.2	82.1	63.0	67.8	80.6
C	73	54.2	62.2	67.7	40.8	46.4	57.7	38.0	44.4	57.4	C	73	68.7	73.4	81.7	74.0	78.1	87.0
C	102	54.2	62.2	67.7	38.3	44.3	58.2	3.9	5.6	11.2	C	102	69.9	75.0	83.9	57.1	63.6	70.6
B	2	43.7	44.7	66.7	31.0	32.4	54.9	35.5	35.7	87.9	B	2	54.6	53.9	84.1	54.1	53.3	84.2
B	3	43.7	44.7	66.7	26.4	27.5	47.5	22.7	23.7	45.0	B	3	63.6	64.4	84.5	49.9	47.8	82.7
B	32	43.7	44.7	66.7	32.4	33.6	56.4	37.2	37.6	87.4	B	32	50.7	49.3	80.8	59.4	60.0	83.4
B	33	43.7	44.7	66.7	32.4	33.6	56.4	22.2	21.0	69.1	B	33	50.7	49.3	80.8	49.1	49.6	74.2
B	47	43.7	44.7	66.7	36.2	38.5	65.7	22.5	25.6	55.9	B	47	48.5	46.8	79.3	22.8	22.8	23.9
B	49	43.7	44.7	66.7	35.8	37.6	63.6	38.8	38.9	95.5	B	49	52.7	52.5	78.9	53.4	53.5	80.1
B	80	43.7	44.7	66.7	34.9	36.0	57.9	39.9	41.2	77.4	B	80	52.4	52.4	78.3	56.7	56.9	85.6
B	82	43.7	44.7	66.7	20.9	21.2	37.6	40.9	42.3	67.3	B	82	45.5	45.2	73.1	47.8	48.3	75.3
B	93	43.7	44.7	66.7	34.9	36.3	59.7	48.2	50.8	82.6	B	93	55.9	56.3	79.7	50.8	50.4	78.4
B	99	43.7	44.7	66.7	32.1	33.8	58.3	1.4	1.8	10.7	B	99	54.5	54.1	83.5	41.4	41.0	69.8
M	5	67.8	61.7	70.3	66.4	59.7	64.7	51.2	44.8	50.2	M	5	85.7	81.6	87.6	72.6	66.1	73.2
M	6	67.8	61.7	70.3	69.9	62.5	68.5	67.7	62.4	110.0	M	6	76.0	73.0	83.2	83.4	78.9	85.4
M	44	67.8	61.7	70.3	68.9	61.4	66.9	67.5	62.0	107.0	M	44	86.4	82.6	87.9	73.8	70.8	80.3
M	46	67.8	61.7	70.3	68.9	61.4	66.9	48.6	45.4	96.8	M	46	89.3	86.5	90.4	75.5	72.1	83.1
M	59	67.8	61.7	70.3	69.3	61.8	66.8	70.3	64.1	96.3	M	59	81.7	76.8	84.4	74.6	70.4	81.9
M	61	67.8	61.7	70.3	69.3	61.8	66.8	45.4	43.4	84.5	M	61	81.7	76.8	84.4	55.9	53.6	73.1
M	62	67.8	61.7	70.3	36.4	31.6	33.1	62.6	55.6	59.9	M	62	79.1	77.4	86.4	43.3	41.7	46.8
M	70	67.8	61.7	70.3	36.6	32.3	36.4	93.9	83.6	88.0	M	70	75.3	70.2	80.5	79.9	74.6	81.7
M	90	67.8	61.7	70.3	76.1	68.9	74.6	34.6	32.7	32.4	M	90	87.4	83.3	87.6	34.5	31.6	26.9
M	96	67.8	61.7	70.3	62.9	56.5	62.6	10.7	8.7	12.9	M	96	87.2	83.7	88.6	75.1	68.8	78.0

HDR and Appearance

Appendix 2-2

		Paint Sample			Scene Radiance						Painting					
					3-D Mondrians			3-D Mondrians			LDR Watercolor			HDRWatercolor		
		Spectrolino			LDR KM100			HDR KM100			Spectrolino			Spectrolino		
W	9	93.2	93.4	92.0	100.0	100.0	100.0	35.5	34.0	53.2	85.7	85.7	71.6	73.3	73.4	74.4
W	24	93.2	93.4	92.0	49.1	49.1	50.2	68.0	68.2	69.5	92.3	92.4	91.5	95.1	94.9	95.9
W	28	93.2	93.4	92.0	49.0	48.8	50.1	57.2	57.2	64.1	93.0	93.0	90.9	87.2	87.6	87.9
W	29	93.2	93.4	92.0	49.0	48.8	50.1	25.2	24.9	29.0	93.0	93.0	90.9	78.4	79.0	81.9
W	57	93.2	93.4	92.0	73.8	73.8	75.6	31.2	31.4	38.5	85.9	85.6	73.3	50.9	51.7	53.3
W	60	93.2	93.4	92.0	39.6	38.3	42.7	100.0	100.0	100.0	84.1	84.8	83.7	88.4	88.7	78.8
W	63	93.2	93.4	92.0	81.4	80.7	78.2	51.3	50.5	45.4	91.1	91.1	83.8	41.4	41.2	39.8
W	81	93.2	93.4	92.0	76.4	76.4	77.5	86.8	87.4	96.3	94.7	94.8	93.4	89.7	89.9	81.3
W	83	93.2	93.4	92.0	76.4	76.4	77.5	51.1	51.5	73.6	94.7	94.8	93.4	75.5	76.5	85.3
W	84	93.2	93.4	92.0	39.6	38.7	40.7	63.0	56.5	60.7	83.0	83.1	81.7	74.1	71.3	78.6
W	85	93.2	93.4	92.0	39.0	38.6	35.6	48.1	46.8	26.1	69.4	64.3	52.4	65.5	61.3	42.5
W	95	93.2	93.4	92.0	80.8	81.0	83.1	16.6	16.6	20.5	95.8	95.9	94.2	89.6	89.8	89.8
NL	1	72.5	73.1	74.6	58.8	59.3	62.6	32.4	32.7	35.3	83.4	83.3	83.0	78.3	78.5	77.3
NL	15	72.5	73.1	74.6	55.6	55.8	58.2	48.0	48.4	51.9	78.7	78.7	78.9	78.7	78.8	76.1
NL	23	72.5	73.1	74.6	39.1	39.2	41.3	61.2	61.5	62.1	73.7	73.9	74.8	74.9	74.9	73.3
NL	26	72.5	73.1	74.6	54.4	54.7	58.2	47.9	49.8	81.9	84.3	84.5	85.3	71.7	72.3	74.8
NL	27	72.5	73.1	74.6	54.4	54.7	58.2	40.1	42.6	81.0	84.3	84.5	85.3	53.8	54.6	59.6
NL	77	72.5	73.1	74.6	45.4	45.7	47.9	69.0	69.7	69.9	71.8	71.8	72.5	68.7	68.8	60.7
NL	78	72.5	73.1	74.6	45.4	45.7	47.9	13.6	13.9	21.9	68.1	68.1	68.8	43.6	44.1	46.1
NL	86	72.5	73.1	74.6	24.7	25.2	26.5	13.0	12.9	13.5	45.3	45.3	46.5	23.8	23.1	22.4
NL	87	72.5	73.1	74.6	63.1	63.7	66.1	25.8	26.5	25.9	96.1	96.2	94.4	29.7	26.6	24.4
NL	101	72.5	73.1	74.6	60.1	60.6	64.0	9.2	9.3	12.8	75.5	75.6	76.3	60.7	60.7	61.9
NM	18	59.5	60.1	61.1	47.8	48.2	49.8	30.8	31.3	45.5	72.3	72.4	73.4	57.8	57.9	53.7
NM	25	59.5	60.1	61.1	36.0	36.2	38.4	26.3	26.4	32.7	82.9	82.8	82.0	61.1	61.0	61.6
NM	34	59.5	60.1	61.1	44.9	45.1	47.0	48.7	50.3	73.6	70.9	70.9	71.7	84.5	84.6	84.3
NM	35	59.5	60.1	61.1	44.9	45.1	47.0	24.8	25.1	30.0	70.9	70.9	71.7	62.2	62.5	65.2
NM	71	59.5	60.1	61.1	28.5	28.1	29.7	26.4	25.7	29.2	58.6	58.6	59.6	51.6	52.7	51.7
NM	72	59.5	60.1	61.1	28.5	28.1	29.7	70.9	71.1	69.9	58.6	58.6	59.6	66.7	66.8	62.4
NM	88	59.5	60.1	61.1	62.5	63.0	65.7	69.1	69.7	68.4	86.8	86.8	86.5	69.2	69.4	64.8
NM	89	59.5	60.1	61.1	62.5	63.0	65.7	20.9	19.7	20.0	86.8	86.8	86.5	65.6	65.7	61.7
NM	104	59.5	60.1	61.1	48.4	48.8	51.3	5.7	5.7	8.3	62.7	62.7	63.9	55.3	55.3	56.9
ND	4	41.0	41.4	43.3	44.1	44.8	50.4	22.8	21.1	45.4	48.2	48.6	51.1	29.7	30.3	32.9
ND	22	41.0	41.4	43.3	18.8	19.1	21.5	23.5	23.9	26.3	45.1	45.1	46.3	50.3	50.2	51.6
ND	36	41.0	41.4	43.3	33.8	33.9	39.3	16.6	16.6	39.2	49.0	49.0	50.3	38.7	38.6	39.9
ND	38	41.0	41.4	43.3	19.4	18.2	18.8	36.2	36.7	38.9	29.6	29.5	30.2	58.6	58.9	62.1
ND	48	41.0	41.4	43.3	28.0	28.4	31.5	39.7	40.4	48.1	26.7	26.5	25.4	51.3	51.2	52.5
ND	98	41.0	41.4	43.3	34.6	35.0	38.2	1.9	2.1	4.5	50.6	50.6	51.8	36.4	36.3	37.6
K	8	26.0	26.0	26.5	35.4	34.6	36.3	28.3	25.9	47.0	31.8	32.2	26.1	32.2	30.5	42.5
K	12	26.0	26.0	26.5	16.8	15.9	18.0	19.7	17.8	22.7	25.1	25.0	24.3	26.5	25.8	26.4
K	21	26.0	26.0	26.5	12.2	11.6	12.1	13.5	10.9	8.9	23.2	22.9	22.4	23.3	23.3	24.4
K	37	26.0	26.0	26.5	19.6	19.6	20.5	12.8	13.0	19.4	23.3	23.1	22.6	25.6	25.4	25.5
K	40	26.0	26.0	26.5	22.8	22.6	22.5	17.9	18.2	23.7	6.2	6.3	12.2	46.1	46.3	33.1
K	41	26.0	26.0	26.5	22.8	22.6	22.5	8.8	9.4	18.2	21.9	21.7	21.2	26.0	25.7	25.4
K	64	26.0	26.0	26.5	14.7	14.6	15.3	26.3	26.0	25.5	25.0	24.7	24.2	32.9	32.8	32.3
K	79	26.0	26.0	26.5	23.2	23.3	24.9	10.6	10.7	15.0	2.1	2.2	3.9	25.4	25.2	24.9
K	94	26.0	26.0	26.5	19.0	19.0	20.7	0.3	0.1	3.2	23.7	23.4	22.9	24.2	23.9	23.3